

SOME ASPECTS OF THE EFFECTS
OF PROPELLER OPERATION ON THE STATIC
LONGITUDINAL STABILITY OF AN AIRPLANE

THESIS

BY

RICHARD W. BELL

HARRISON A. STORMS, JR.

IN PARTIAL FULFILLMENT OF THE
REQUIREMENTS FOR THE DEGREE OF AERONAUTICAL ENGINEER
CALIFORNIA INSTITUTE OF TECHNOLOGY
PASADENA, CALIFORNIA

1941

TABLE OF CONTENTS

	<u>Page</u>
Acknowledgement	1
Index of Figures	2
Notation	6
Model Geometry	9
Introduction	10
Description of Tests	12
Preliminary Discussion of Power-on Effects	16
Empirical Results Relating to the Five Models Tested	23
Concluding Remarks	41
References	43
Experimental Curves and Figures	44

ACKNOWLEDGEMENT

The authors wish to express their appreciation for the advice given them by Dr. Clark B. Millikan throughout the preparation of the material presented here. They also extend thanks to those aircraft companies, and their representatives, whose close cooperation made these investigations possible.

Index of Figures

1. Six component setup for ten foot wind tunnel tests at the Galcit.
2. Geometrical comparison of the five airplanes.
3. Tail - slipstream relationship.
4. Tail pitching moments power-on and power-off for four different stabilizer settings. - Airplane No. 1
5. Tail pitching moment power-off and power-on with three rotations, plotted in families of constant τ_c for two stabilizer settings. - Airplane No. 2
6. Tail pitching moment power-off and power-on with three rotations, plotted in families of consistent rotation for two stabilizer settings. - Airplane No. 2
7. Tail pitching moments power-on and power-off for three different stabilizer settings. - Airplane No. 3
8. Power-off tail pitching moment for four elevator settings. - Airplane No. 4
9. Power-on tail pitching moment for four elevator settings, plotted in families of consistent rotation. - Airplane No. 4
10. Tail pitching moments power-on and power-off for three different stabilizer settings. - Airplane no. 5
11. Comparison of lift curve slopes as a function of τ_c for the five airplanes.

12. Comparison of stabilizer effectiveness for the five airplanes and three rotations.
13. Comparison of $\partial C_p / \partial \alpha$ as a function of τ_c for the five airplanes and three rotations.
14. Comparison of tail pitching moment slopes as a function of τ_c for the five airplanes and three rotations.
15. Height of slipstream center line above the thrust axis, taken at the elevator hinge line, plotted vs. α with τ_c as a parameter. - Airplane No. 1
16. Height of slipstream center line above the thrust axis, taken at the elevator hinge line, plotted vs. α with τ_c as a parameter. - Airplane No. 2
17. Height of slipstream center line above the thrust axis, taken at the elevator hinge line, plotted vs. α with τ_c as a parameter. - Airplane No. 3
18. Height of slipstream center line above the thrust axis, taken at the elevator hinge line, plotted vs. α with τ_c as a parameter. - Airplane No. 4
19. Height of slipstream center line above the thrust axis, taken at the elevator hinge line, plotted vs. α with τ_c as a parameter. - Airplane No. 5
20. The percentage of the tail area covered by the slipstream, ϕ , plotted as a function of α for the various τ_c 's. - Airplane No. 1
21. The percentage of the tail area covered by the slip-

- stream, ϕ , plotted as a function of α for the various $Tc's$. - Airplane No. 2
22. The percentage of the tail area covered by the slipstream, ϕ , plotted as a function of α for the various $Tc's$. - Airplane No.3
23. The percentage of the tail area covered by the slipstream, ϕ , plotted as a function of α for the various $Tc's$. - Airplane No. 4
24. The percentage of the tail area covered by the slipstream, ϕ , plotted as a function of α for the various $Tc's$. - Airplane No. 5
25. The variation with thrust of $\eta_e^p / \eta_t \neq A_p$ for the five airplanes and three rotations.
26. The variation with thrust of the downwash increment due to power, for the five airplanes and three rotations.
27. The variation B_p with T_c for the five airplanes and three rotations.
28. Experimental and calculated values of pitching moment increment due to propeller rotation for the tail removed configuration.
29. Experimental and calculated values of δC_{mw}^p , the pitching moment increment due to power, tail removed, for airplanes 1 and 2 and three rotations.

30. Experimental and calculated values of $\delta^P C_{mw}$, the pitching moment increment due to power, tail removed, for airplanes 3, 4, and 5 and three rotations.
31. The propeller normal force function, K , plotted verses C_P/J for various values of dC_P/dJ
32. The form of the function ϵ_i/α_t
33. The form of the function ψ
34. The form of the function φ
35. The form of the function. $(1 + \frac{8QT_c}{\pi})$

TABLE I

NOTATION

A	=	Aspect ratio of the wing
A_P	=	Power-on averaging factor
a_{cl}	=	Slope of the lift curve for complete airplane
a_{tcl}	=	Ideal slope of the tail lift curve
B_P	=	Power-on downwash factor
a_a	=	Wing chord behind center line of propeller
C_L	=	L/q_s , lift coefficient
C_D	=	D/q_s , drag coefficient
C_m	=	M/q_s , pitching moment coefficient
c	=	Wing m.a.c.
d	=	Propeller diameter
h_s	=	Height of slipstream above the thrust axis
h_t	=	Height of tail above the thrust axis
i	=	Wing incidence
i_t	=	Stabilizer setting
K	=	Normal force function
l_1	=	Distance from propeller disk to wing c.p.
l_2	=	Distance from wing c.p. to elevator hinge line
m	=	Power-off downwash factor
Q	=	Percentage of the horizontal tail covered by slipstream

- $q = \rho_2 V^2$, dynamic pressure, free stream
 $q_t = \frac{\rho_2}{2} V_t^2$ dynamic pressure over the tail
 $R = 1 + \frac{ST_c}{\pi}$
 $A =$ Distance from plane of symmetry to thrust line
 $S_w =$ Wing area
 $S_t =$ Tail area
 $T_c = \frac{T}{\rho V^2 d^2}$
 $T'_c = \frac{T}{g s}$
 $x =$ Distance from propeller disk to wing c.p.
 $z =$ Number of propellers operating
 $\alpha =$ Angle of attack of the airplane
 $\alpha_t =$ Angle of attack of the thrust axis
 $V =$ Velocity of flight
 $x_T =$ Distance from C.G. to propeller disk
 $z_T =$ Distance from C.G. to thrust axis
 $\Lambda =$ Empirical constant between 1 and 2, depending upon aspect ratio of wing portions covered by the slipstream
 $\epsilon_p =$ Power-on total downwash at the tail
 $\epsilon_i =$ Inclination of slipstream downstream from propeller disk
 $\epsilon_w =$ Inclination of wing downwash downstream from wing c.p.

Interference factor

() \hookrightarrow Complete model

()_w \hookrightarrow Complete airplane minus tail

()_t \hookrightarrow Tail surfaces

()_T \hookrightarrow Thrust axis

()_p or ()^p \hookrightarrow Power-on

δ = Increment due to the tail

δ_p = Increment due to power.

$$\delta = \frac{Q R (R-1)}{1 + Q (R-1)}$$

TABLE II
GEOMETRY OF THE MODELS TESTED

<u>Airplane No.</u>	<u>1</u>	<u>2</u>	<u>3</u>	<u>4</u>	<u>5</u>
<u>Item</u>					
Taper Ratio	2.08	2.3	2.4	3.0	3.08
l/c	2.60	2.96	2.89	3.16	3.58
l_1/c	1.905	.812	.882	.681	.848
l_2/c	3.975	2.98	2.91	3.085	3.739
s_t/s	0.191	.217	.283	.217	.192
b_t/b	0.374	.316	.288	.352	.274
d/c	1.576	1.390	1.385	1.319	1.47
h_t/c	0.211	.224	.486	.684	.06
c_a/c	1.305	1.110	1.095	1.115	1.18
x/c	1.334	.809	.892	.671	.881
x_t/c	1.532	.77	.884	.734	.882
z_t/c	0.125	-0.109	-.041	-.233	.019
Δ/c	0	.981	1.10	1.08	1.326
z	1	2	2	2	4
$\beta @ .75 R$	38°	23°	29.5°	23°	28°
Dihedral (wing) degrees	5	5	4.5	4.7	3.26
Dihedral (tail) degrees	0	0	12	10	5
i	1°	3°	3°	3°	1.5°

Some Aspects of the Effects
of Propeller Operation on the Static
Longitudinal Stability of an Airplane

I. Introduction

This thesis is to be considered a continuation of the material presented in the paper by Dr. C. B. Millikan, "The Influence of Running Propellers on Airplane Characteristics",¹ and of the work done in the thesis² by Mr. S. E. Belsley on the same subject. In reference 1 Dr. Millikan has derived expressions for the prediction of the power-on effects, dependent upon empirical expressions for the power-on downwash at the tail, and the tail efficiency in the slipstream. In reference 2 Mr. Belsley has put these same expressions in forms which permit experimental determination of the two empirical factors dealing with downwash and tail efficiency power-on. It is in part the purpose of this thesis to present numerical results for these factors, determined empirically from tests run at the Galcit* 10' wind tunnel on five different airplanes. In addition there is presented

*Guggenheim Aeronautics Laboratory, California Institute of Technology.

a discussion of the effects on pitching moment of various rotational configurations for twin-engine monoplanes including the effects on the tail removed configuration. There has appeared in power model testing of multi-engined airplanes the existence of favorable rotational configurations giving better power-on stability than the other possible rotations. As a consequence two of the five airplanes were tested for three different rotational configurations. The experimental data have been reduced in a manner that demonstrates clearly the effect of rotation alone on pitching moment. Unfortunately, similar data could not be obtained on the other airplanes, due to the limited time available for research at the Galcit tunnel.

II. Description of the Tests

Tests were conducted on the five airplane models which are described in the following general manner:

1. Single-engined low-wing monoplane.
2. Twin-engined mid-wing monoplane.
3. Twin-engined high-wing monoplane with very high tail.
4. Twin-engined mid-wing monoplane with high tail.
5. Four-engined high-wing monoplane.

These tests were made in the Galcit 10' wind tunnel (Fig. 1), and were carried out in the normal manner of procedure at the Galcit. Lift, drag and pitching moment measurements were taken as functions of the uncorrected angle of attack with respect to the direction of flow in the tunnel. These quantities were then reduced to the dimensionless coefficients C_L , C_D , and C_M , and were corrected for wind tunnel wall interference to the corresponding free stream values. Tests were made power-off and power-on for the complete model minus the tail, and for the complete model including the tail for various stabilizer settings. The difference between the drag readings power-off and power-on

was taken as a measure of the thrust

$$T_c' = (C_D)^P - C_D$$

from which the thrust coefficient T_c is given by the equation

$$T_c = \frac{S}{2Zd^2} T_c'$$

All power-on tests were run at as nearly constant T_c vs. α as possible, since the methods of references 1 and 2 depend upon constant thrust polars.

The procedure for operating at constant T_c consisted of maintaining constant electrical power input to the model electric motors. The resulting thrust obtained was constant over the required range of angle of attack within engineering accuracy. The tests run at zero thrust, ($T_c = 0$), were made by matching the power-off drag polar, C_D vs. C_L . The windmilling polars were taken with no power input to the motor.

There resulted, then, for each complete test a family (with T_c as parameter) of lift vs. α curves, and a family of pitching moment vs. lift curves for the two configurations:




- (1) The tail-off configuration.
- (2) The tail-on configuration for each stabilizer setting.

The difference between (2) and (1) above, taken at constant angle of attack, is the increment in pitching moment due to the tail. The families of tail pitching moment curves so obtained are plotted on Figs. 4 - 10, where $\delta_x^P C_M$ and $\delta_x C_M$ are plotted against the lift coefficient for the complete airplane with thrust and stabilizer setting as the parameters. From Figs. 4 - 10 can be derived the empirical quantities necessary for the determination of the downwash and tail efficiency factors. (cf. Section IV A)

In the case of the single engined airplane tested the direction of propeller rotation was right-handed, or clockwise looking forward. In the case of the four-engined airplane, the direction of rotation of each of the four propellers was also right-handed. However, in the case of the twin-engined airplanes, several different rotational configurations were used. On airplanes Nos. 2 and 4, three rotations were tested. The procedure in taking data was the same as described above in the case of each rotation.

The notation used to describe these rotational configurations is the normal notation used at the Galcit.

The letter P denotes propeller in operation, the subscript 1 or 2 denotes the left or right hand propeller respectively, and the subscript R or L denotes right or left-handed rotation respectively in the same sense as described above. Then the configurations tested were as follows:

1. $P_{1R} P_{2R}$  ("up in the middle")
2. $P_{1L} P_{2R}$  ("down in the middle")
3. $P_{1R} P_{2L}$  ("up in the middle")

On airplane no. 3 only the configuration $P_{1L} P_{2R}$ was tested.

III. Preliminary Discussion of Power-on Effects.

The complex effects which running propellers have upon longitudinal stability may be listed under three headings in the following manner:

A. Effects on the tail:

1. The increase in tail efficiency due to slipstream velocity and interference.
2. The effect upon downwash over the tail due to the presence of the slipstream.

B. Effects upon wing-fuselage combination:

1. Moments produced by the direct propeller forces and moments.
2. Moments produced by increments of wing lift and moment due to the slipstream.

C. Destabilizing effect due to rotational components in the slipstream.

1. Effect, both on the tail and on the wing-fuselage combination, of unfavorable rotational configurations for multi-engined airplanes.
2. Effect on the tail-off configuration with propellers running at zero thrust.

Those effects listed under A and B have been treated analytically. The rotation effects listed under C

could as well be listed in A and B, but since they cannot at the present time be set up analytically, they are best considered separately. All three effects will be considered in detail in Section IV of the thesis.

Dr. Millikan, in reference 1, has suggested a procedure for setting up the static longitudinal stability power-on. The fundamental steps involved are outlined in the following discussion. Adopting the same notation as that used in reference 1, the lift and moment power-on will be given by

$$C_L^P = C_{LW} + \delta_P C_{LW} + \frac{g_e^P}{g} \frac{S_t/S}{1/c} C_{Lt}^P \quad (1)$$

$$C_M^P = C_{MW} + \delta_P C_{MW} - \frac{g_e^P}{g} \frac{l/c}{S_t/S} C_{Lt}^P \quad (2)$$

where C_{LW} , and C_{MW} are the lift and moment power-off, tail-off and $\delta_P C_{LW}$ and $\delta_P C_{MW}$ are the increments due to power, tail-off. The remaining terms give the lift and moment contributed by the tail, power-on.

The contribution to lift, $\delta_P C_{LW}$ can be considered as the combination of two terms:

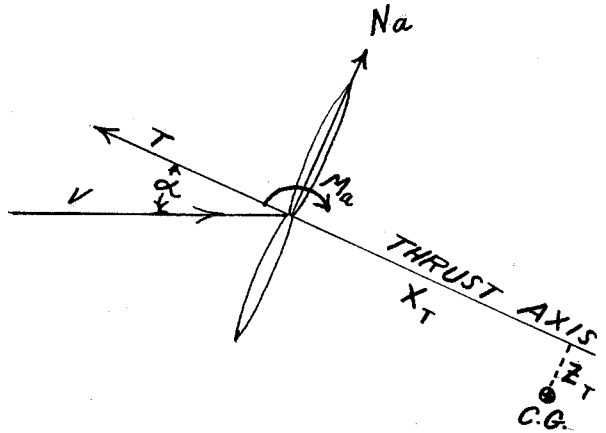
(1) the component of thrust acting in the lift direction

$$C_i = \frac{2Zd^2}{S} T_c \alpha_a \quad (3)$$

and 2) the lift due to interaction of slipstream and wing

$$\delta C_L = \frac{z d^2}{s c} \sqrt{\frac{1+\mu}{1+s}} (\lambda C_{l_0} - K_2 \alpha_a) \quad (4)$$

The contribution $\delta_P C_{M_W}$ represents the effects under heading B at the beginning of the section. The moments due to direct propeller forces, thrust and normal force can be written as follows:



$$(\delta_P C_{M_W})_{PROP} = \frac{2 z X_T d^2}{c s} \left[2 \frac{z_I}{X_T} T_c + K \alpha_a \right] \quad (5)$$

where the function

$$K = .365 \left[\frac{C_P}{J} - \frac{1}{2} \frac{d C_P}{d J} \right]$$

is Glauerts expression for the normal propeller force.

(cf. Fig. 31) The moment M_a is negligible. The moment produced by wing lift and moment increments can only be very roughly approximated analytically. As suggested by Dr. Millikan, an indication of what might be expected is given by the expression

$$(\delta_P C_{M_W})_{INTERFERENCE} = \delta C_L \left[\frac{C_s}{c} \frac{C_{M_W}}{C_{L_W}} + \frac{h}{c} \right] \quad (6)$$

where C_{M_W} AND C_{L_W} are taken power-off, tail-off,

C_S = average wing chord in slipstream

h = distance of aerodynamic center of C_S
ahead of C. G.

As shown in Figs. 28 - 30, the interference effects are noteworthy.

The moment contributed by the tail, power-on, is chiefly influenced by the tail efficiency and the downwash at the tail. These are given in Dr. Millikan's paper as functions of the empirical constants A_P and B_P . The relation of these constants to the efficiency and downwash can be derived as follows:

1) The tail lift coefficient power-on is defined as

$$C_{L_t}^P = J_t^P a_{t_i} (\alpha_P - \epsilon_P + i_t - i_P)$$

where J_t^P is an interference or averaging factor. Reference 1 assumes that the ratio of the average dynamic pressure over the tail, power-on, to the free stream dynamic pressure is given by

$$q_t^P / q = 1 + \frac{8QT_c}{\pi}$$

where Q = fraction of tail in slipstream.

Then the tail efficiency, power-on, will be defined by

$$\eta_t^P = \frac{S_t^P}{S_t} \frac{g_t^P}{g} = S_t^P \left(1 + \frac{B_Q T_c}{\pi}\right)$$

Since the efficiency power-off is defined in a similar manner

$$\eta_t = S_t \frac{g_t}{g}$$

we find the ratio of the two efficiencies to be

$$\frac{\eta_t^P}{\eta_t} = A_P \left(1 + \frac{B_Q T_c}{\pi}\right) \quad (7)$$

where $A_P = \frac{S_t^P}{S_t} / \frac{g_t}{g}$, can be regarded as an empirical

"power-on averaging factor" to be evaluated. (cf. Section IV)

2) The downwash increment due to power has been defined thus: the total downwash power-on is the sum of the power-off downwash plus the increment due to power:

$$\epsilon_P = \frac{m C_{LW}}{\pi A} + f_D \alpha_P + g_D$$

where m = power-off downwash factor $\doteq 2$ and f_D , g_D are functions of T_c and an empirical constant, B_P , which give the downwash increment as a function of the power-on lift coefficient, since

$$\alpha_P = \alpha_P(C_L^P=0) + a_P C_L^P$$

It has been assumed that

$$g_D = f_D (i_w - i_p)$$

and that f_D will be given according to the expression

$$f_D = \frac{B_P Q R (R-1)}{1 + Q (R-1)} \quad (8)$$

where

Q = fraction of tail in slipstream

$$R = 1 + \frac{8 T_c}{\pi}$$

B_P empirical constant to be evaluated

(cf. Section IV A)

This completely defines the downwash and tail efficiency power-on since A_P and B_P are free to absorb deviations from the theory. If A_P and B_P are known, the tail pitching moment can be computed by the method of reference 1. The propeller forces are presumably known and hence their effect is readily computed by equation (5). There remain only the interference effects due to slipstream velocity and rotation. The relative order of magnitude of these effects can be determined for the five airplanes tested from Figs. 28 - 30 and Figs. 4 - 10. The effects are quite large in some cases. The authors have attempted to isolate as many of the effects as possible, with the view of obtaining some consistent

explanation of the effects. However, the number of tests obtained was not sufficient to give anything but the types of interference to be found, which are in some cases quite unexpected. The following section deals with the results of the experiments in detail.

IV. Empirical Results Relating to the Five Models Tested

A. Tail Efficiency and Downwash, Power-on; the Determination of A_p and B_p

In the previous section was shown the relation of the empirical constants A_p and B_p to the tail efficiency, η_t^p , and the downwash factor f_d . As mentioned in the test procedure the tests on all five models were carried out specifically to enable the evaluation of those experimental quantities necessary for computation of A_p and B_p . The method used to reduce the data so obtained is that derived in reference 2. The fundamental quantities required were the slope of the lift curve power-on and power-off, tail pitching moment slopes and stabilizer effectiveness, and the change in zero lift intercept with stabilizer angle. These are compared for the five airplanes in Figs. 11-14. The tail pitching moment curves of the five airplanes are plotted in Figs. 4 - 10.

The relationships necessary for the computation of A_p and B_p are listed below in the notation of Reference 2. (cf. Table I)

From reference 2

Power-off

$$m = \pi A \left[\frac{1}{a} - \frac{\beta \gamma}{\nu} \right] \quad (9)$$

$$\frac{1}{\eta_t} = \frac{S_t}{S} a_{ti} \left[\frac{1}{a} - \frac{\beta \left(\frac{l}{c} + \gamma \right)}{\nu} \right] \quad (10)$$

Power-on

$$f_D = \frac{\nu}{\gamma} \frac{\left[1 - \frac{m}{\pi A} (a_P - \omega) \right] - a_P \left[1 - \beta \left(1 + \frac{m \omega}{\pi A} \right) \right]}{\frac{\nu}{\gamma} + a_P \beta} \quad (11)$$

$$\frac{1}{\eta_t^P} = \frac{S_T}{S} a_{ti} \frac{\left[\frac{m}{\pi A} - \frac{l}{c} \frac{1}{\gamma} \left(1 - \frac{\beta m}{\pi A} a_P \right) \right]}{\frac{\nu}{\gamma} + a_P \beta} \quad (12)$$

where $\omega = \frac{Z d^2}{S} \left[2 T_c + K_1 (1 + a_w - K_2) \right]$

A_P and B_P are given in terms of these quantities
by

$$A_P = \frac{\eta_t^P}{\eta_t} \left/ 1 + \frac{\beta Q T_c}{\pi} \right. \quad (13)$$

$$B_P = f_D / \varphi \quad (14)$$

where
$$\phi = \frac{QR(R-1)}{1 + Q(R-1)}$$
 (cf. Fig. 34)

Fundamental to the determination of A_p and B_p is the adoption of some logical definition of the percentage of the tail covered by the slipstream. We shall refer to this percentage as Q . In reference 1 Q was defined as that portion of the tail falling between two concentric cylinders passing downstream from the propeller, of radii equal to 20% and 80% of the propeller radius. Preliminary investigations showed, however, that Q computed on this basis for airplanes Nos. 3 and 4 is very nearly zero. Moreover, it appeared from wake surveys made at the Galtit 10' wind tunnel that Q based upon full propeller diameter would more accurately represent conditions at the tail. Were the actual position of the slipstream at the tail known for a given angle of attack and thrust, this definition would give a satisfactory value of Q . Therefore, the authors made calculations for the theoretical position of the slipstream center line at the tail.

In reference 3 Glauert gives a theoretical expression for the inclination of the slipstream behind an inclined propeller. Denoting the slipstream inclination by ϵ , and

the inclination of the propeller by α_T , then Glauert's expression is

$$\frac{\epsilon_1}{\alpha_T} = \frac{2a(1+a)(1 + \frac{K}{T_c})}{(1+2a)[1 + a(1 + \frac{K}{T_c})]} \quad (15)$$

where

$$2a = -1 + (1 + \frac{8T_c}{\pi})^{1/2}$$

Fig. 35

$$K = .365 \left[\frac{C_P}{J} - \frac{1}{2} \frac{dC_P}{dJ} \right]$$

Fig. 31

On Fig. 32, ϵ_1/α_T is plotted as a function of T_c for various values of K . The inclination of the wing downwash is given in T. R. 648 for various values of aspect ratio and taper ratio. Derived from the empirical data given there, the function Ψ has been plotted in Fig. 33, where Ψ is such that the inclination of the wing downwash power-on or power-off is given by

$$\begin{aligned} \epsilon_w &= \Psi C_L \\ \epsilon_w^P &= \Psi C_{L,}^P \end{aligned} \quad (16)$$

where

$$C_{L,}^P = C_L^P - T_c' \alpha_T$$

We denote the distance from the plane of the propeller to the center of pressure of the wing as l_1 , and the distance from the center of pressure of the wing to the hinge line of the elevator as l_2 . We further

assume that wing downwash and propeller downwash at the tail are additive. Then the slipstream inclination downstream from the propeller disk will be given by ϵ_1 , between disk and wing C.P., and by $\epsilon_1 + \epsilon_w^P$ between the wing C.P. and the elevator hinge line. (cf. Fig. 3) Therefore, the expression giving the height of the slipstream center line above the thrust axis at the elevator hinge line may be written

$$h_s = (l_1 + l_2) \tan \alpha_t - l_1 \tan \epsilon_1 - l_2 \tan (\epsilon_1 + \epsilon_w^P)$$

or for small angles this becomes, from equations (15) and (16)

$$\begin{aligned} h_s &= (l_1 + l_2) (\alpha_t - \epsilon_1) - l_2 \epsilon_w^P \\ h_s &= (l_1 + l_2) \alpha_t \left(1 - \frac{\epsilon_1}{\alpha_t}\right) - l_2 \psi C_L^P \quad (17) \end{aligned}$$

Using the experimental values of C_L^P obtained in the test, this function was computed for each of the five airplanes. The results are plotted on Figs. 15 - 19, showing h_s at the elevator hinge line plotted against angle of attack for various values of T_C . (solid lines). The horizontal dashed line in the figures represents h_r , the vertical location of the elevator hinge line with respect to the extended thrust axis. The dashed circles in the figures represent the propeller disk, centered at h_r on the vertical axis. A point on the solid curves gives h_s for a given α and T_C . The distance between the dashed circle and the h_s axis, taken at the same value of

gives the value of the half-chord of the slipstream cylinder which intersects the plane of the tail at the given α and T_c . Therefore, the span of the tail immersed in the slipstream is at once apparent and values of Q can be computed for each angle of attack. In Figs. 20-24 are plotted the values of Q calculated in this manner for the models tested.

It would appear that the above method is only a rough approximation since interference effects have been neglected. In the case of single-engine airplanes there is large interference between slipstream and fuselage. In the case of multi-engine airplanes there is interference with the wing-nacelle combination, and a tendency for the slipstream to swing to one side or the other of the thrust axis depending upon the rotation used, and upon the geometry of the wing-nacelle combination. The results obtained, however, based on this Q , give gratifying justification of the method used. Furthermore the results for h_s check fairly closely with wake tests made at the Galcit on airplane No. 3.

On Fig. 25 are plotted the tests results for η_t^p / η_t vs T_c for all five airplanes. Referring to equation (13), p. 24, we see that empirical values of A_p will be given by

$$A_P = \frac{\eta_t^P}{\eta_t} / 1 + \frac{8Q\tau_c}{\pi}$$

(For the meaning of A_P refer to Section III)

where Q is determined from Figs. 20-24, (having been computed according to the method outlined above). The values of A_P computed by this relationship are plotted on the same figure. (Fig. 25) We see that, with one exception, equation (13) gives nearly constant values of A_P over the range of τ_c 's considered. The variation of η_t^P/η_t as a function of τ_c for all five airplanes is matched so well by the loading

$$R = 1 + \frac{8Q\tau_c}{\pi}$$

that the quotient, A_P , is constant within 5% deviation from the mean value 1.0. In other words, the power-on tail efficiency may be computed within 5% error for most cases by the expression

$$\eta_t^P = A_P \left(1 + \frac{8Q\tau_c}{\pi} \right) \eta_t$$

where

$$A_P = 1$$

As might be expected from the preceding discussion, the actual percentage of the tail covered by the slipstream may differ for different rotational configurations. Since the Q that we compute does not take these rotational effects into account, we may expect differences between the rotations in the values of A_P based on this Q .

Reference to Fig. 25 shows that such differences do occur. For airplane No. 2 the differences between rotations is not very large. Hence Q must not change much with rotation for this airplane, as is verified later by the results for the downwash at the tail. However, for airplane No. 4, there is a large difference in A_P between "down in the middle" and "up in the middle" rotations. Since all three rotations for this airplane give values of A_P that are too high, there must be some general interference effect that renders the Q calculation slightly in error. However, only "down in the middle" rotation is beyond limits of error, indicating that this rotational configuration covers more of the tail than was predicted, i.e. converges toward the fuselage. This agrees with the observed tendencies for this rotation with large underslung nacelles. In the same way we note that for airplane No. 3, tested only for "Up in the middle" rotation, the values of A_P are low, although within limits of error. This indicates divergence of the slipstreams away from the fuselage, as has been observed for large underslung nacelles.

We may conclude that for most cases, single-engine, or multi-engine with favorable rotation, A_P may be taken as constant and equal to 1.0

It is of some interest to consider the slipstream

positions plotted in Figs. 15-19. For airplanes Nos. 1, 2 and 5 the tail is in the slipstream by almost the same amount for all values of τ_c and angle of attack. For airplanes Nos. 2 and 4 the tail, due to its height, is just entering the slipstream at negative angles of attack, and the amount of the tail in the slipstream is approximately some linear function of τ_c and α . This is of interest in the discussion that follows.

On Fig. 26 is plotted the variation of the downwash factor, f_D , as a function of τ_c for the various airplanes tested. The factor, f_D , gives the downwash increment due to power according to the equations on pp. 20-21, Section III. The values on Fig. 26 were obtained from empirical data using the method of reference 2 (equations, p. 24). The results again show highly interesting rotational effects.

By equation (17) the inclination of the slipstream center line must always be downward. Yet, in Fig. 26 there appears negative downwash increment due to power. The curves of all three rotations for airplane No. 2 have negative intercepts. This can, perhaps, be laid to experimental error. The other effects of rotation on the slope and values of f_D vs. τ_c cannot, however, be ignored. These effects can be interpreted in the following manner. It has been shown by wake tests that the rotational com-

ponents in the slipstream give a tremendous variation in the downwash angle over the span of the tail, (of the order of 6° to 10°). This variation, however, must be a function of the position of the slipstream with respect to the tail. It must also be a function of the rotational configuration. Then, if the center of the slipstream lies on the tail for all values of T_c and angles of attack, as is the case for airplanes 1, 2, and 5, we would expect variation in downwash increment due to power, depending upon the rotational configuration, as follows: (assuming the tail extends outboard of the nacelles)

- 1). "Up in the middle" rotation moves the slipstreams outboard on the tail, resulting in less average downwash than if the slipstream went straight back.
- 2). "Down in the middle" rotation moves the slipstream inboard, resulting in more average downwash than for a straight slipstream.

Now suppose that the slipstream falls well below the tail and that the tail span lies between the thrust axes. Then the tail area covered by the slipstream, as in airplanes 3 and 4, is no longer constant. For "up in the middle" rotation we might well expect an upwash increment due to the upward component of the inboard half of the slipstream.

This upwash will increase with τ_c , due to increasing rotational speed, provided that the slipstream does not fall off the tail with increasing τ_c . For "down in the middle" rotation we would expect less upwash increment than if the slipstream went straight back, due to the divergence of the slipstreams.

Considering Fig. 26 again, we see that this reasoning is consistently born out. For airplane No. 2 Q is practically constant (cf. Fig. 21). The span of the twin tail used in the tests extended beyond the thrust axis. From Fig. 26 we see that there is a variation in the slope, $\frac{df_b}{d\tau_c}$, the slope and the downwash being greatest for "down in the middle" rotation. The difference in downwash between rotations is not as great, however, as that for airplane No. 4. Here a high single tail empennage was tested, the span of the horizontal tail extending only as far as the thrust axis. Note that the difference in downwash between convergent and divergent rotations is very large, again consistent with the interpretation. Airplane No. 3 was unfortunately tested only with the configuration "up in the middle". This is the most interesting result, however, since the increment is entirely upwash, f_b increasing negatively as τ_c increases. The empennage tested with this airplane was set high above the thrust axis, (cf. Fig. 22), and its span extended outboard only as far as the thrust line. A large propeller diameter

was used, resulting in larger Q than for the airplane No. 4. Therefore, for the divergent rotation tested, the increment due to the propeller was upwash, increasing with T_c . This checks with the preceding interpretation for high tail position.

It is suggested that further checks on the effects of propeller operation might be made by varying J at constant values of T_c .

On Fig. 27 are plotted the values of B_p , computed according to equation (14). It was the purpose of this part of the investigation to determine whether the function

$$f_D = \varphi B_p \quad (\text{cf. Ref. 1})$$

$$B_p = \text{constant}$$

$$\varphi = \frac{Q R (R-1)}{1 + Q (R-1)} \quad (\text{cf. Fig. 34})$$

was a satisfactory expression for the downwash increment due to power, i.e. to determine whether

$$B_p = f_D / \varphi$$

(f_D and φ from experimental data)

is a constant for all airplanes. The results on Fig. 27 show that for airplanes 2 and 5, and for "up in the middle" rotation of airplane No. 4, a good average value for B_p is 0.20 or 0.30. This is in the neighborhood of values

suggested in references 1 and 2. For the rest of the airplanes and rotations, however, there is considerable deviation in values of B_p . Therefore it appears that the above expression for B_p is not complete. It may hold for certain cases or configurations, but not for all. The preceding discussion has shown that f_b is a function not only of T_c and Q , but also of the rotational configuration and the location of the tail with respect to the thrust axis. A satisfactory function for f_b in terms of these parameters has not yet been derived. It is hoped that future tests in combination with the results presented here will lead to such an expression, either empirical or analytical.

B. Tail-off Pitching Moments, Power-on.

The pitching moment increments due to power, with the tail removed, are plotted in Figs. 28-30 for the five airplanes. The broken lines are the calculated values for the increments in moment due to the thrust and the normal force on the propeller. The calculations are based on the equation

$$\left(\delta^P C_{M_w}\right)_{\text{PROPELLER}} = \frac{2Z X_T d^2}{S} \left[-\frac{Z_T}{X_T} T_c + K \alpha_T \right] \quad (18)$$

where the function K , Glauert's normal force function, has been plotted in Fig. 31. The solid lines on the figures 28-30 are the experimental values of the pitching moment increments. According to equation (18), T_c will introduce a constant moment increment for curves of $\delta^P C_{M_w}$ taken at constant T_c , and the slope of the curve is a function only of the normal force on the propeller, and is always positive. In Figs. 29 - 30 these increments were taken at constant angle of attack of the model in the tunnel. In Fig. 28 both experimental and empirical data were taken at constant C_L , since for zero thrust the lift, propeller running, is approximately the same as the lift, power-off.

The data presented in Fig. 28 represents to a close

approximation the effect on pitching moment due to propeller rotation alone; i.e. for zero thrust. The technique for running zero thrust polars is given in Section II. For airplanes 2 and 3 the curves are for zero thrust. For airplanes 4 and 5 the curves are for wind-milling propellers, since the difference between windmilling and zero thrust polars was found to be negligible. The dashed curves for these cases were computed using the propeller drag increment as negative τ_c . For airplane 1 no zero thrust or windmilling data was taken on the tail-off configuration. The curve presented is at very low thrust, however. For all the airplanes the destabilizing effect due to rotation ranged from 2% to 3% C.G. shift, based on tail-off C_L . The effect was largest on airplane No. 1 because of the large value of χ_T .

For airplane 1 the agreement between calculated and experimental values of the above effect is excellent. Here the instability is due entirely to the normal force on the propeller. The destabilizing effect on the complete airplane is approximately 0.04 for low powers. One-third of this effect is due to interference on the tail, as shown in Fig. 4. The rest of the effect is the normal force on the propeller. For the higher powers the normal force

function does not give the complete effect, predicting higher destabilizing effects than were actually obtained (cf. Fig. 29). Interference effects account for the discrepancy.

For the multi-engined airplanes the propeller force accounts roughly for about half of the destabilizing effect at zero thrust. Presumably the rest is due to rotation interference with the nacelle-wing combination. Referring to Fig. 28, for airplane No. 4, the "rotation up in the middle" has the least interference effect by 50%, and agrees fairly closely with the normal propeller force. However, for airplane No.2 the rotation effects were all practically the same.

The increments in tail pitching moment at high powers for the multi-engined airplanes show various amounts of interference. For airplane No.5 the thrust line lay only 1.9" above the center of gravity. Hence the calculated values for various T_c 's lie very close together, increasing negatively with T_c . This same variation with T_c occurs on the experimental curves but the spread, due to interference, is much greater.

For airplane No. 4 the experimental results are roughly the same for every rotational configuration.

The distance from thrust line to C.G. was quite large in this case, hence the moment increment due to thrust is quite large. The calculated values account for approximately 75% of this thrust increment, and for nearly all of the pitching moment slope. Hence, in this case, also, the destabilizing effect is caused entirely by the normal force on the propeller.

Airplane No. 2 has most peculiar experimental results. The effects for the rotation "up in the middle" are matched very satisfactorily by the calculated values. For all three rotations the destabilizing effect is due to the normal force on the propeller. The increment due to thrust, however, which matches so well for $P_{1L} P_{2R}$, decreases steadily as we pass to the rotation $P_{1R} P_{2R}$, and to $P_{1R} P_{2L}$. This indicates that there exists an interference effect of a nature similar to the effect of rotational configuration upon the flow over the tail. Since this effect is not substantiated by the tests on airplane No. 4, it is difficult to draw definite conclusions from the airplane.

Comparison of the geometrical aspects of the two airplanes reveals no pertinent difference, except in

the size of the airplanes, that might explain the appearance of the effect. No. 4 has 3 thrust line incidence with respect to the wing, and has shorter, fatter nacelles than those of No. 2. Both airplanes are mid-wing, having the same airfoil section, with large under-slung nacelles. The propeller diameters and the distance of the thrust axes from the plane of symmetry are proportional for both airplanes. The size and general dimensions of the fuselages are proportional.

However, the effect joins with the other rotational results too well to be disregarded, having once appeared. Further tests, with extensions in the isolation of effects, such as polars at various values of J for constant τ_c , may help to determine when and why such an effect occurs. It is suggested that if possible, tests be made on a very simple wing-nacelle combination, in an attempt to determine not only rotational effects, but also the effect of the vertical position of the thrust axis on wing-nacelle interference and the downwash behind the wing.

V. Concluding Remarks

The following conclusions may be drawn from these investigations:

- 1). The "power-on averaging factor", A_p , has an average value of unity. The power-on tail efficiency is therefore satisfactorily expressed as a function of the disk loading, $B\tau_c/\pi$, and the percentage of the tail in the slipstream, Q

$$\eta_t^p/\eta_t = 1 + BQ\tau_c/\pi$$

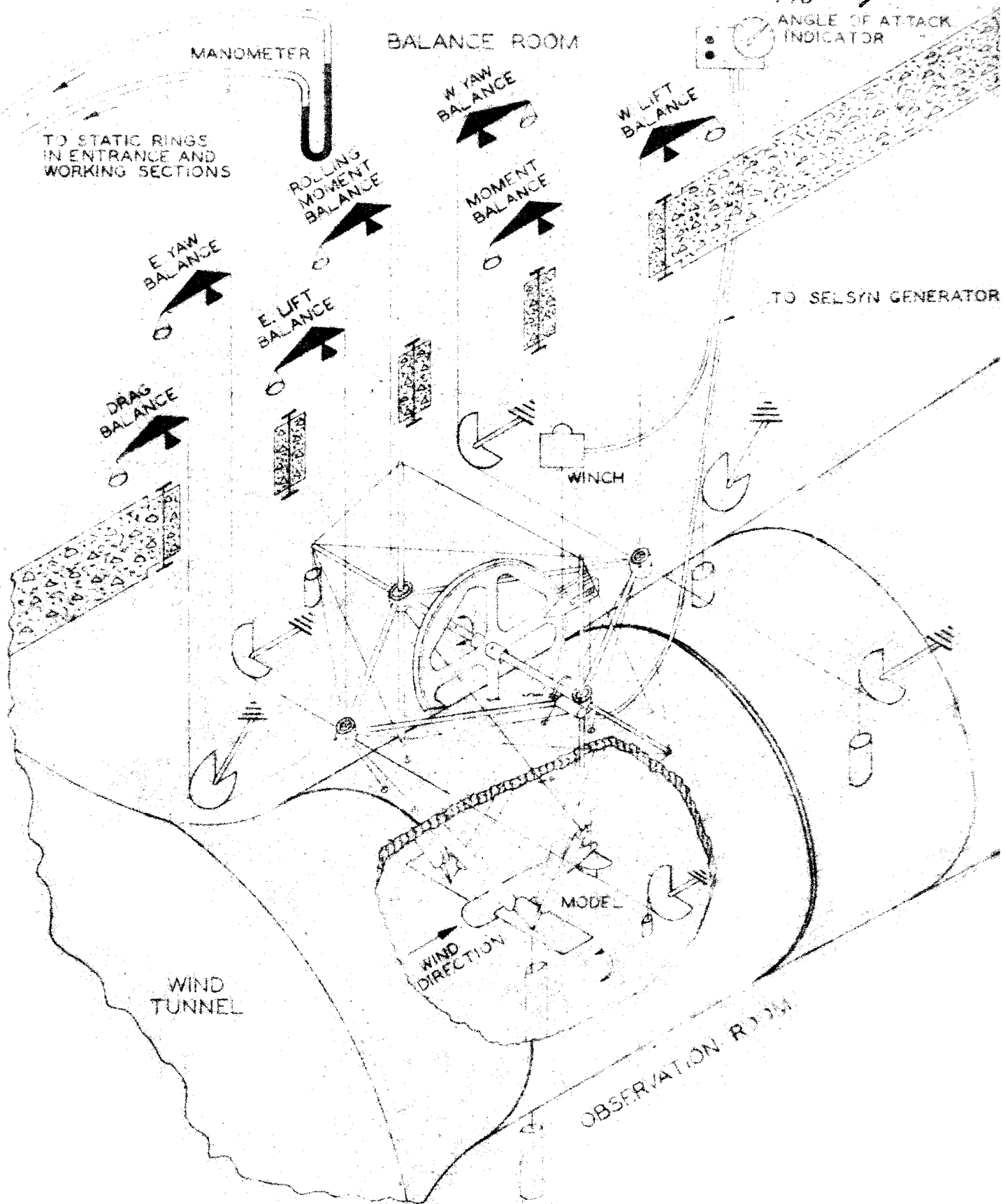
- 2). The path of the slipstream can be approximated by the sum of propeller downwash and wing downwash, permitting a consistent evaluation of Q .
- 3). The average downwash at the tail is not only a function of τ_c and Q , but also is directly and largely effected by propeller rotation and the airplane geometry. The results show that the downwash cannot be approximated by a constant value of B_p . For normal tail positions and rotations, B_p has the value 0.30 as suggested in Reference 1.

However, for unfavorable rotations and high tail positions, values of B_p diverge greatly from this value (cf. Fig. 27). This indicates that the analysis needs further reduction or division to take into account this rotational and geometrical effect.

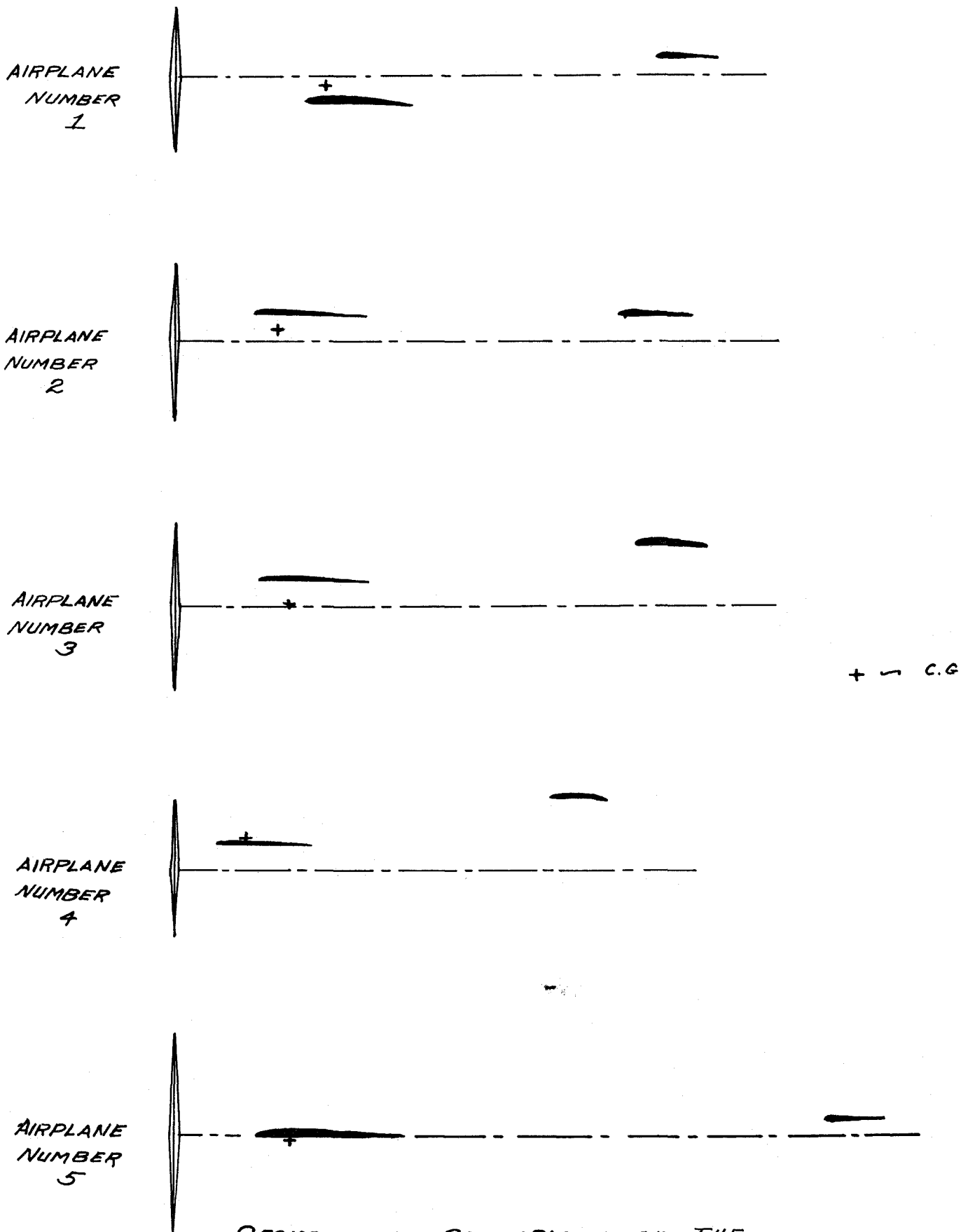
- 4). Interference effects on the wing-fuselage or wing nacelle combinations are large. The relative magnitude of these effects may possibly depend upon the rotational configuration used. In some cases the effect of this interference in stability is negligible, the normal propeller force giving the total destabilizing effect due to power on the tail-off configuration. The inconsistency of these effects warrants further investigation.

REFERENCES

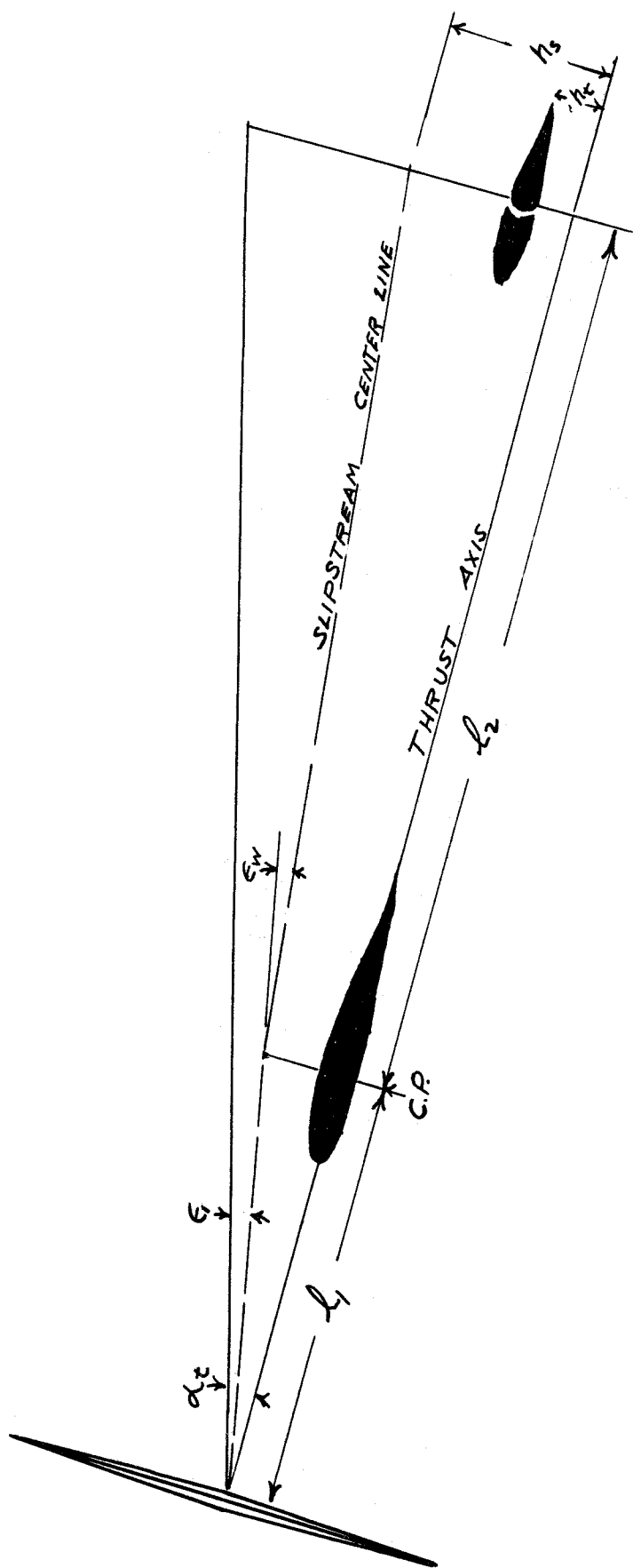
- 1) Millikan, C. B., The Influence of Running Propellers on Airplane Characteristics, Journal of the Aeronautical Sciences, Jan. 1940.
- 2) Belsley, S. E., Determination of Two Parameters Dealing with Power-on Stability for a Model with Right-hand Propellers, Calif. Instit. of Tech., June, 1940.
- 3) Glauert, Miscellaneous Airscrew Problems, Durand, vol. IV, page 359.
- 4) Silverstein A., and Katzoff, S., Design Charts for Predicting the Downwash and Wake Behind Plane and Flapped Wings, N.A.C.A. Tech. Rep. 648, 1939.
- 5) Glauert, H., Stability Derivatives of an Airscrew, British Aero. Res. Com. Reports and Memoranda, No. 642, 1919.
- 6) Lesley, E.P., Worley, G. F., and Moy S., Air Propellers in Yaw, N.A.C.A. Tech. Rep. 597, 1937.
- 7) Gates, S.B., A Survey of Longitudinal Stability Below the Stall, with an Abstract for Designers Use, Reports and Memoranda No. 1118, 1927.



SIX COMPONENT SETUP FOR TEN FOOT WIND TUNNEL TESTS
AT GUGGENHEIM AERONAUTICS LABORATORY
CALIFORNIA INSTITUTE OF TECHNOLOGY

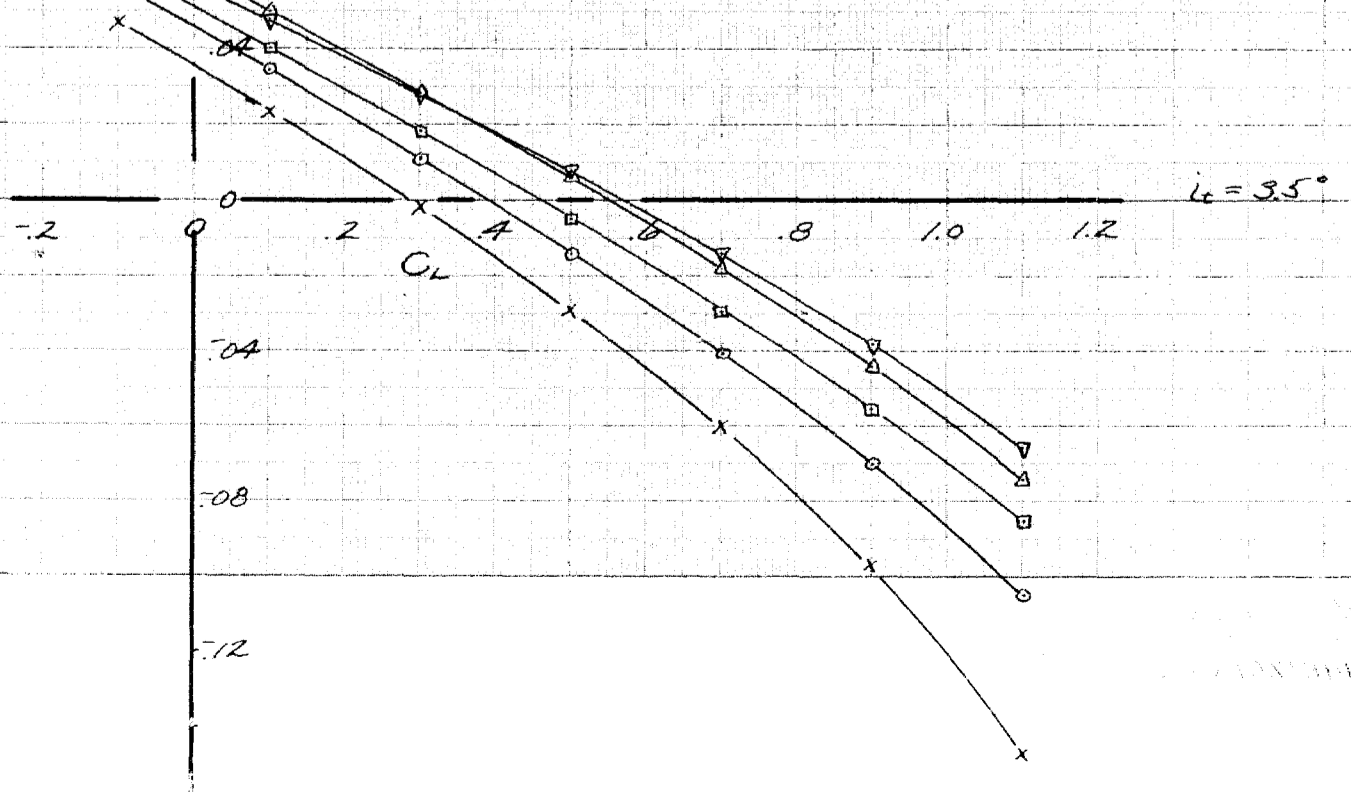
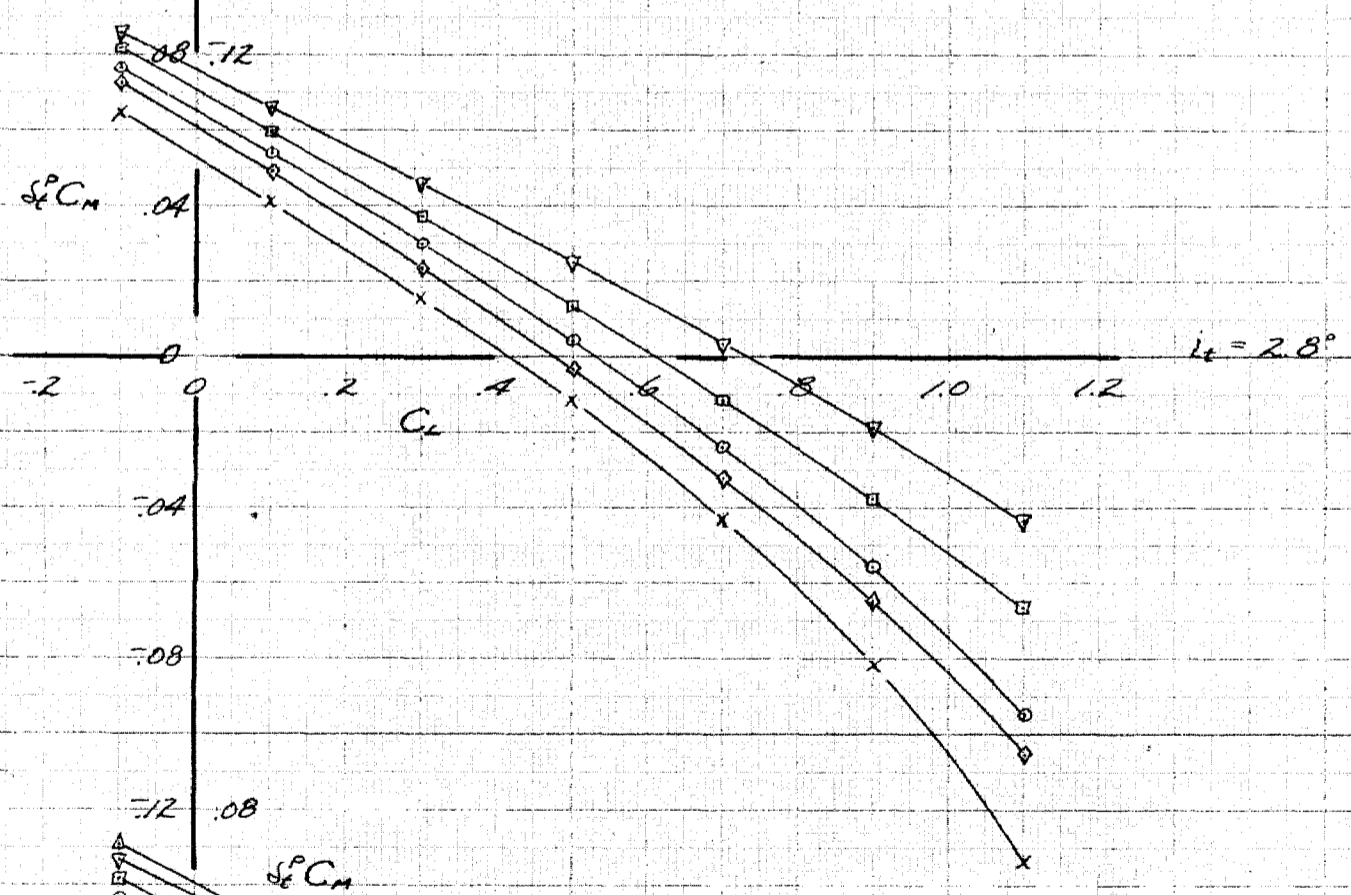
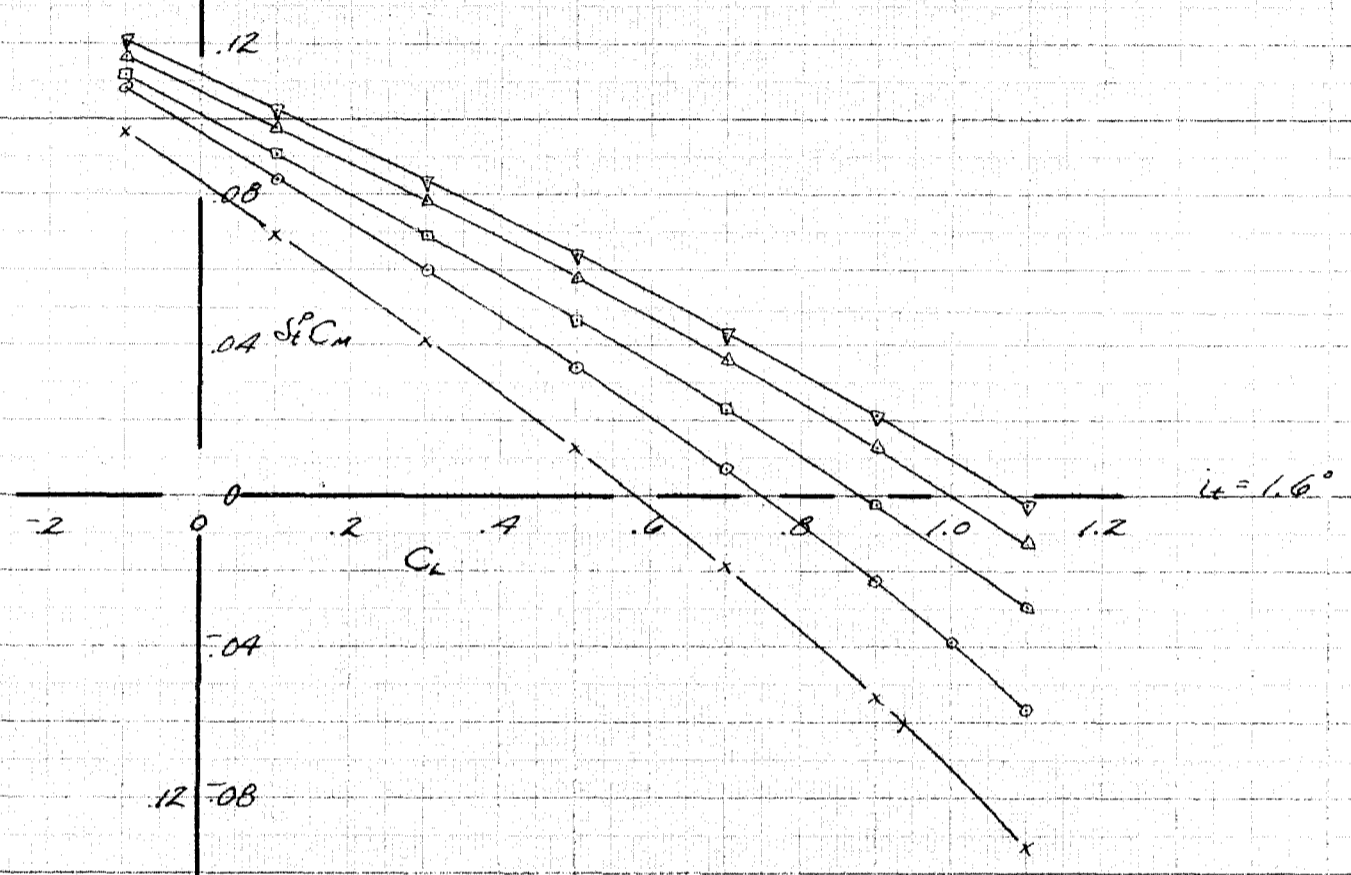
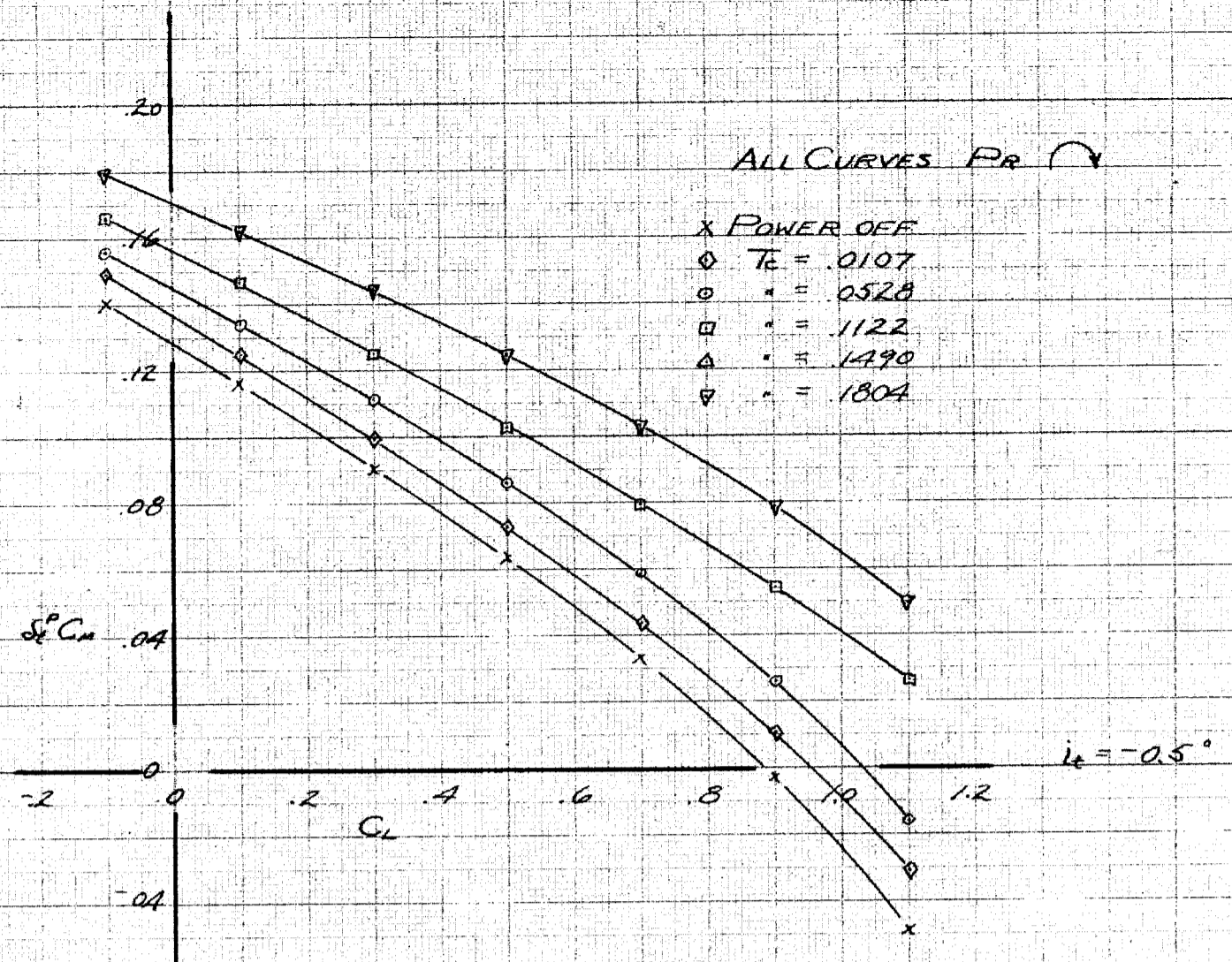


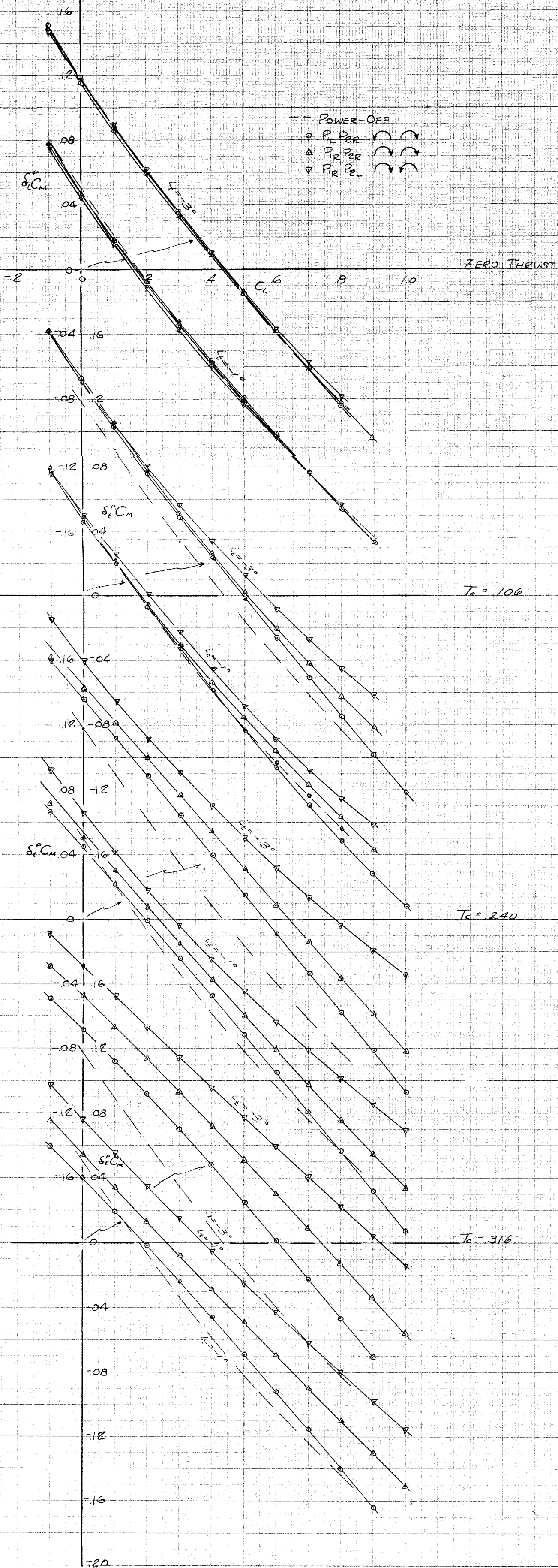
GEOMETRICAL COMPARISON OF THE
FIVE AIRPLANES



TAIL SLIPSTREAM RELATIONSHIPS

TAIL PITCHING MOMENTS POWER ON AND POWER OFF
FOR FOUR DIFFERENT STABILIZER SETTINGS
AIRPLANE NO. 1



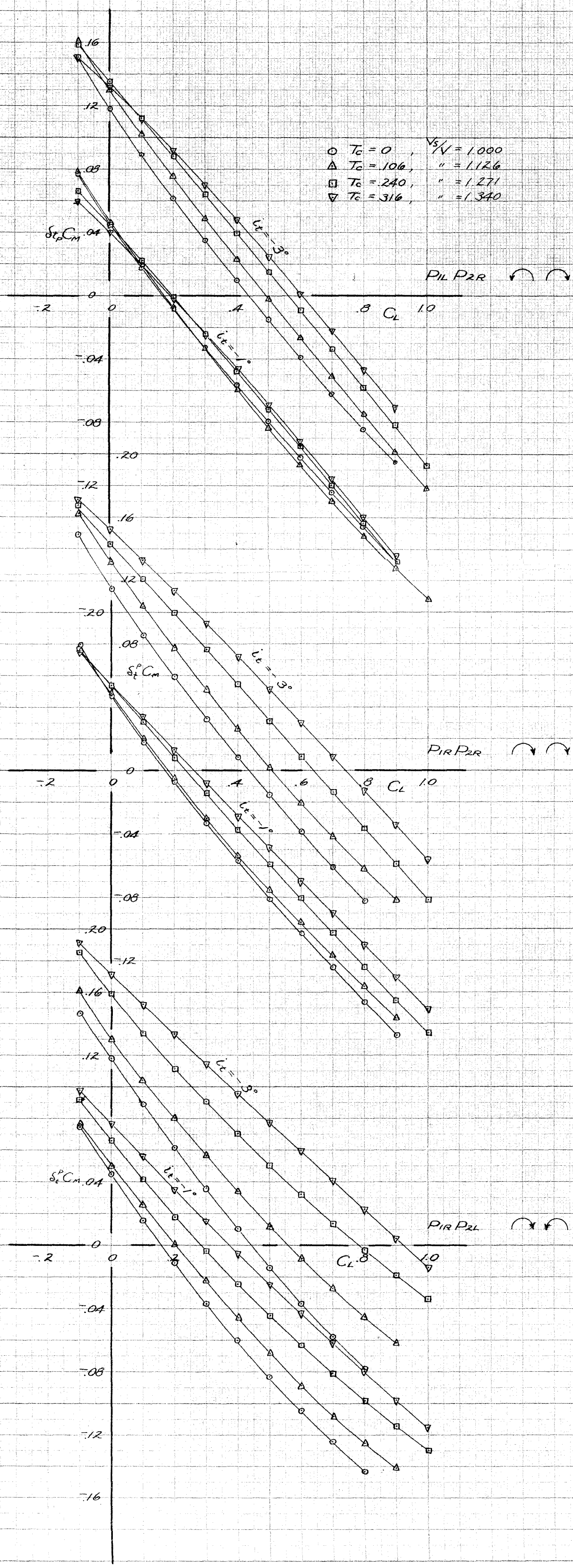


TAIL PITCHING MOMENT POWER-OFF AND POWER-ON
WITH THREE ROTATIONS, PLOTTED IN FAMILIES OF
CONSTANT T_c FOR TWO STABILIZER SETTINGS

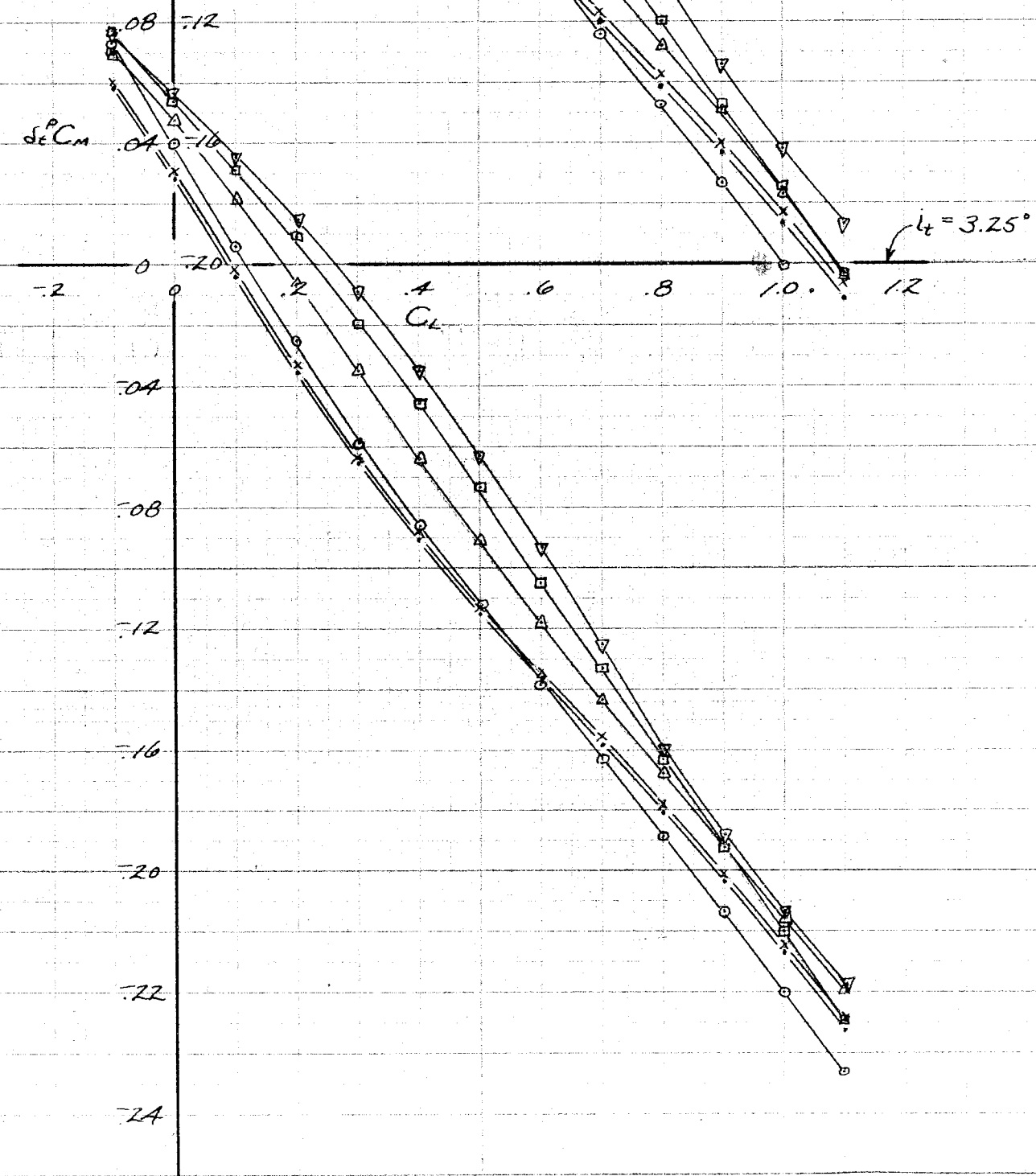
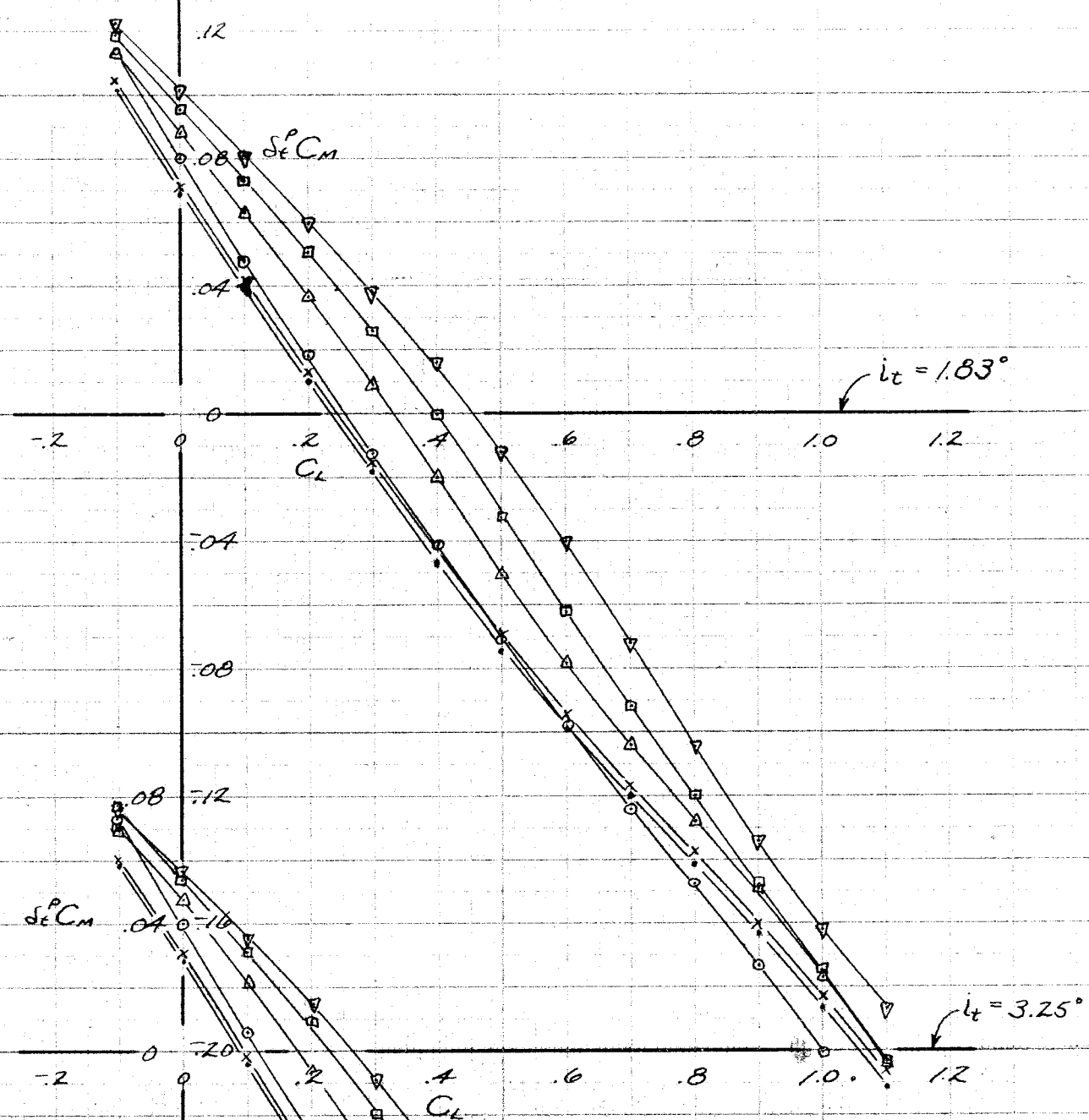
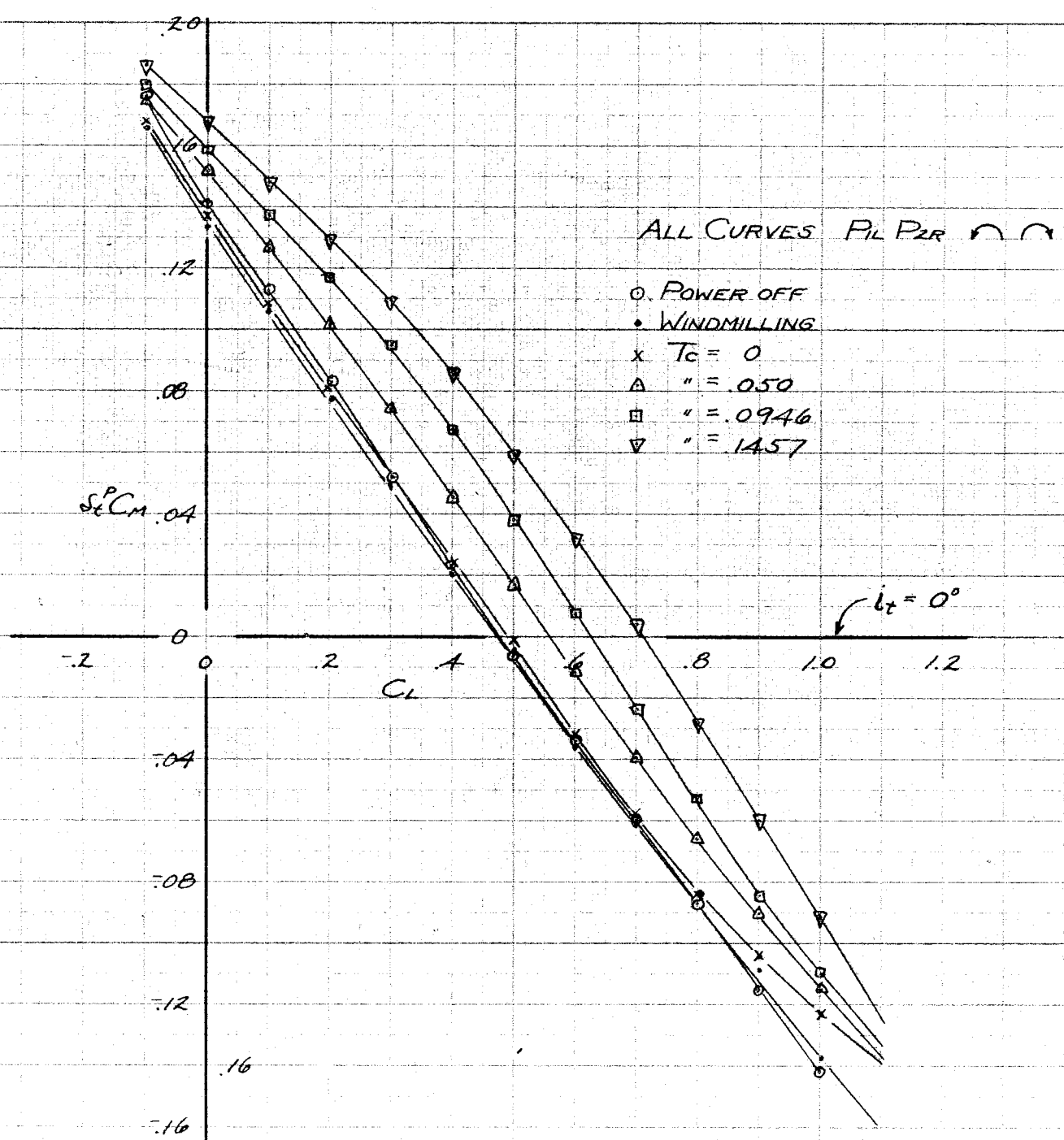
AIRPLANE NO. 2

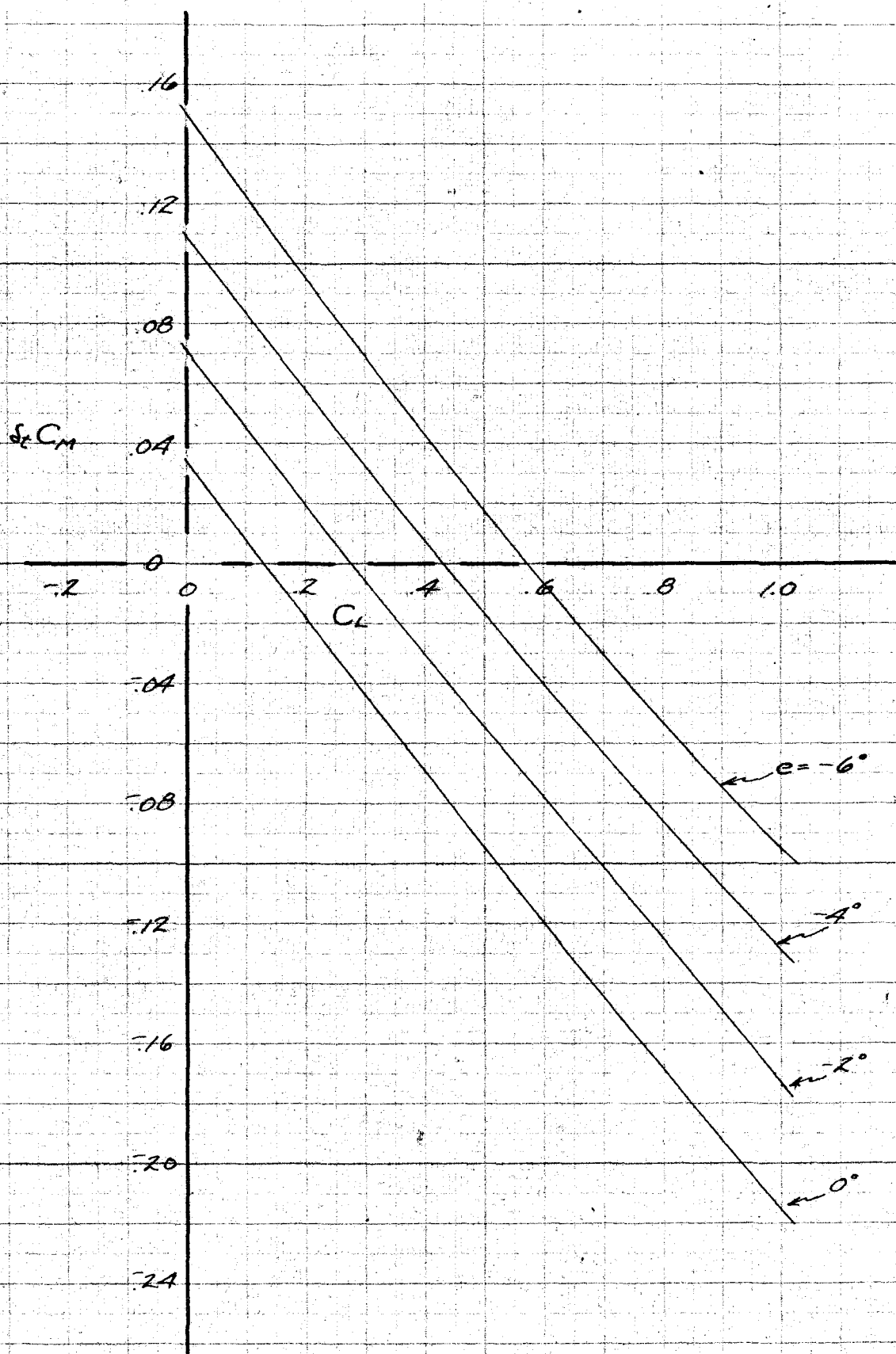
TAIL DITCHING MOMENTS, POWER-OFF AND POWER-ON
WITH THREE ROTATIONS, PLOTTED IN FAMILIES OF
CONSISTENT ROTATION FOR TWO STABILIZER
SETTINGS

AIRPLANE No. 2



TAIL PITCHING MOMENTS POWER-ON AND POWER-OFF
FOR 3 DIFFERENT STABILIZER SETTINGS
AIRPLANE NO. 3

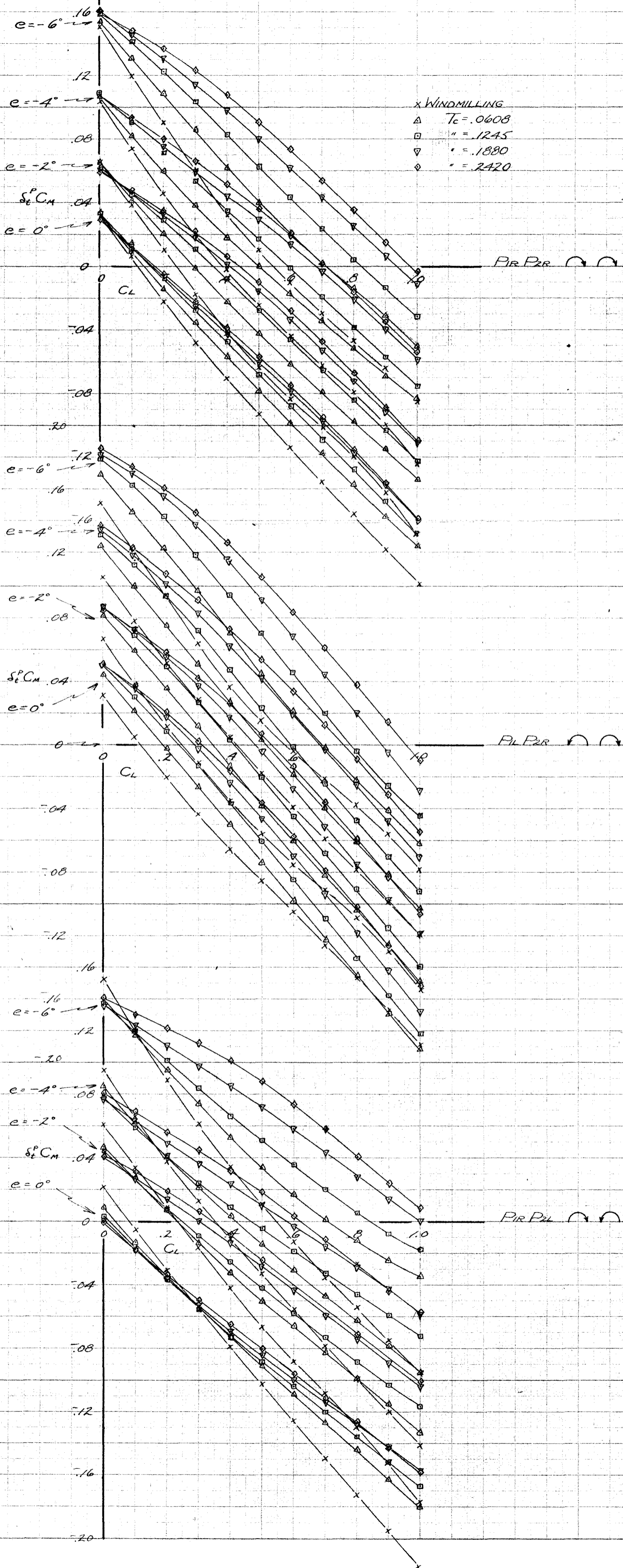




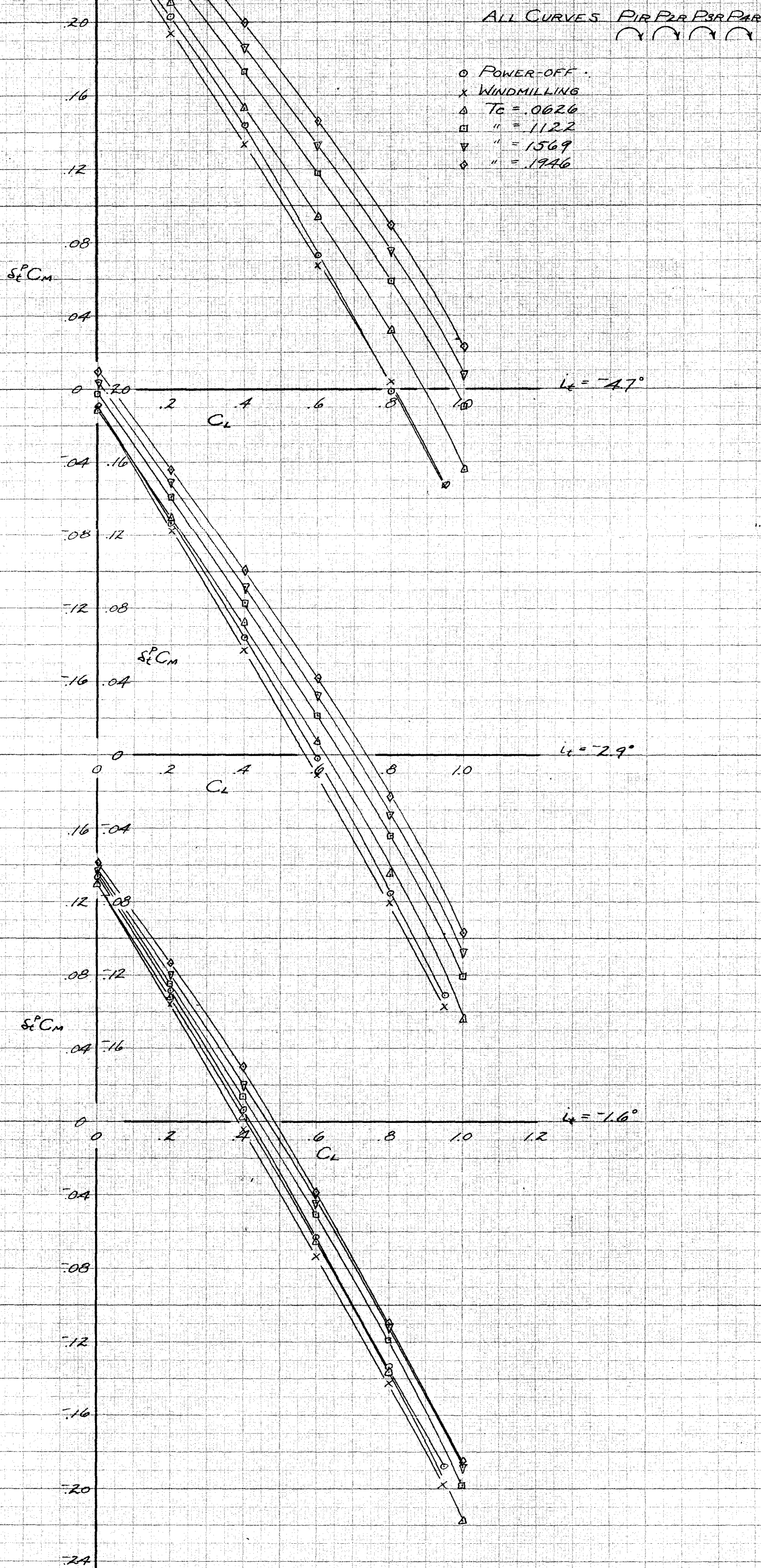
TAIL PITCHING MOMENTS, POWER OFF, FOR 4
ELEVATOR SETTINGS

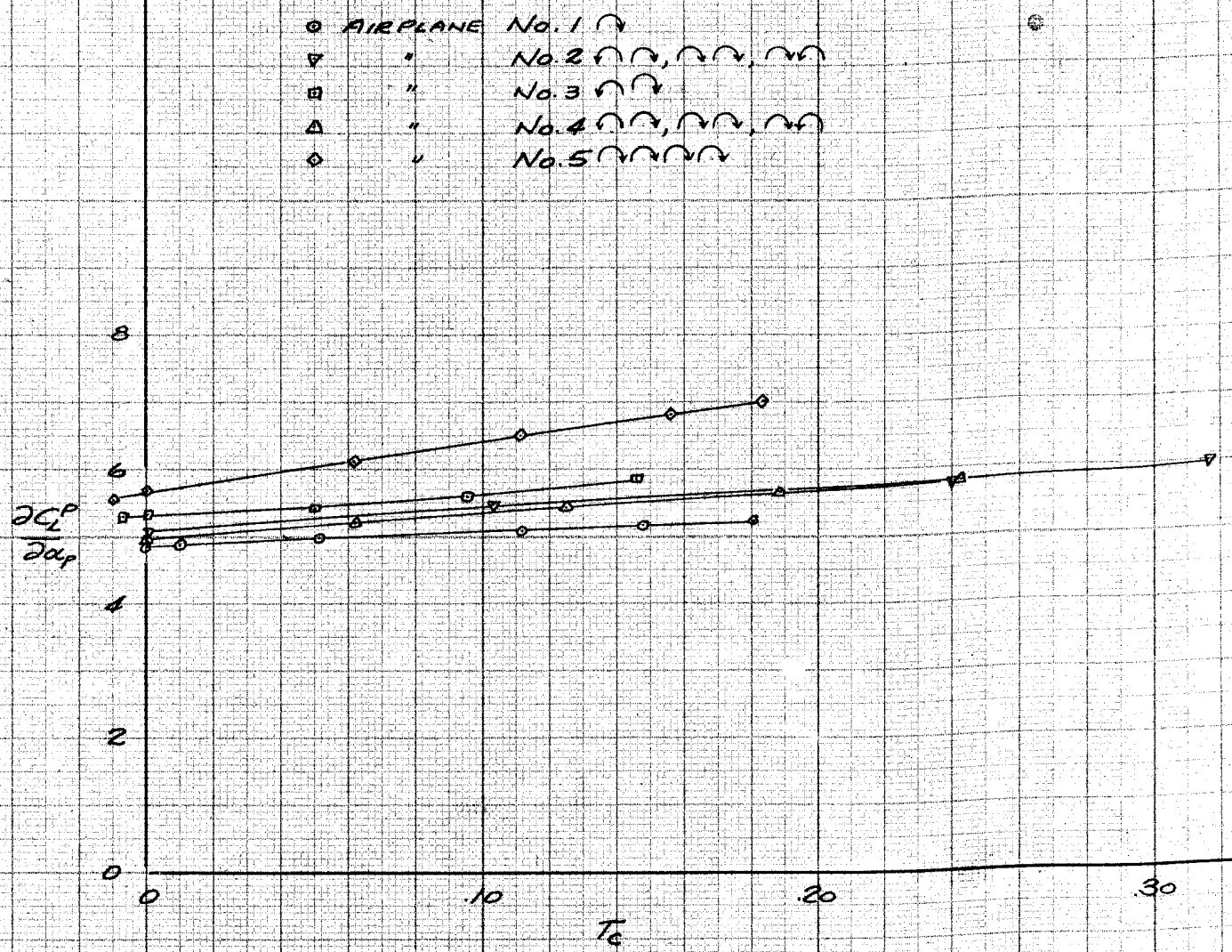
AIRPLANE No. 4

TAIL PITCHING MOMENTS, POWER-DOWN, FOR 4 ELEVATOR
SETTINGS PLOTTED IN FAMILIES OF CONSISTENT
ROTATION
AIRPLANE NO. 4

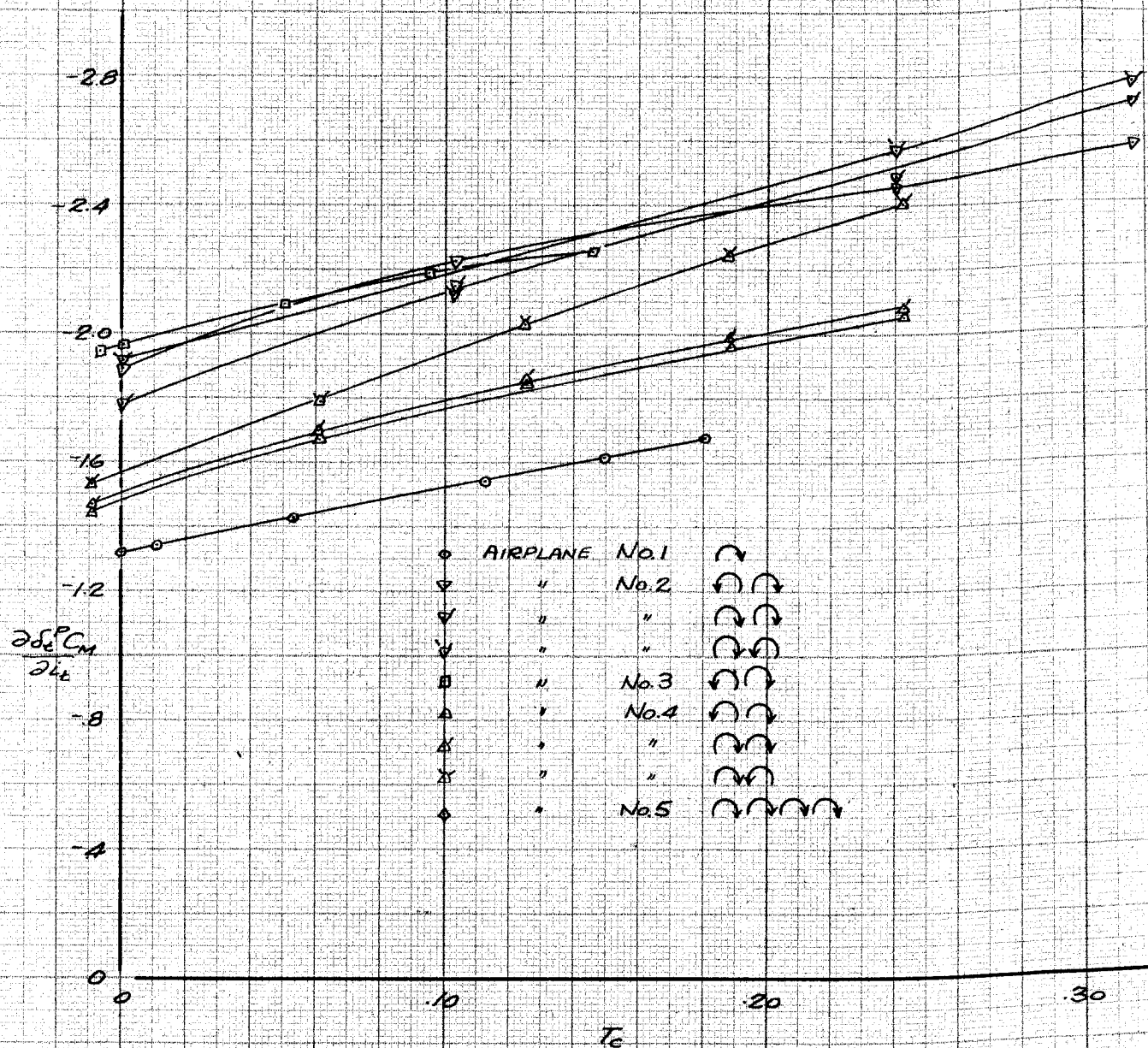


TAIL PITCHING MOMENTS POWER-ON AND POWER-OFF
FOR THREE DIFFERENT STABILIZER SETTINGS
AIRPLANE NO. 5



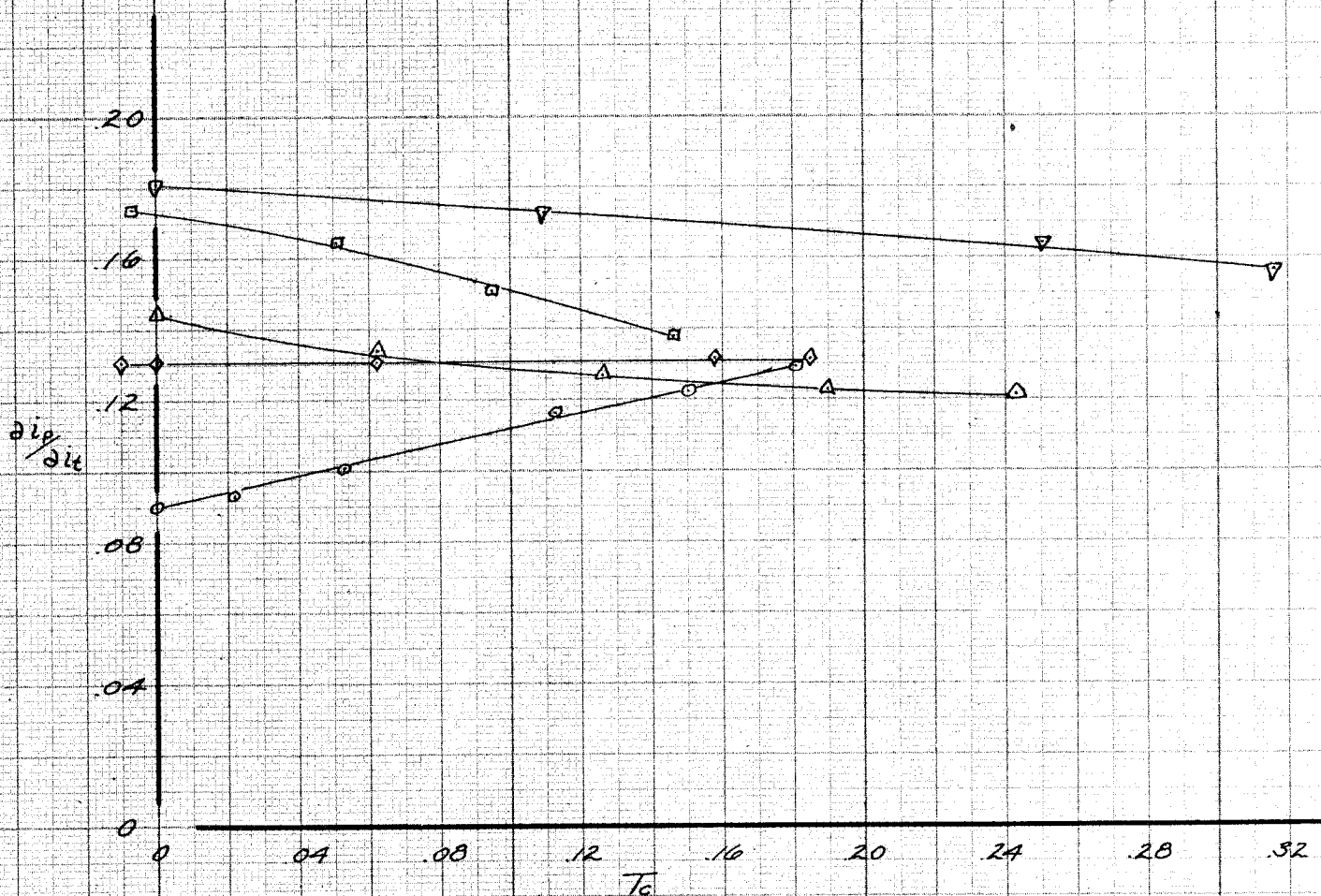


COMPARISON OF LIFT CURVE SLOPES AS A FUNCTION OF T_c
FOR THE FIVE AIRPLANES



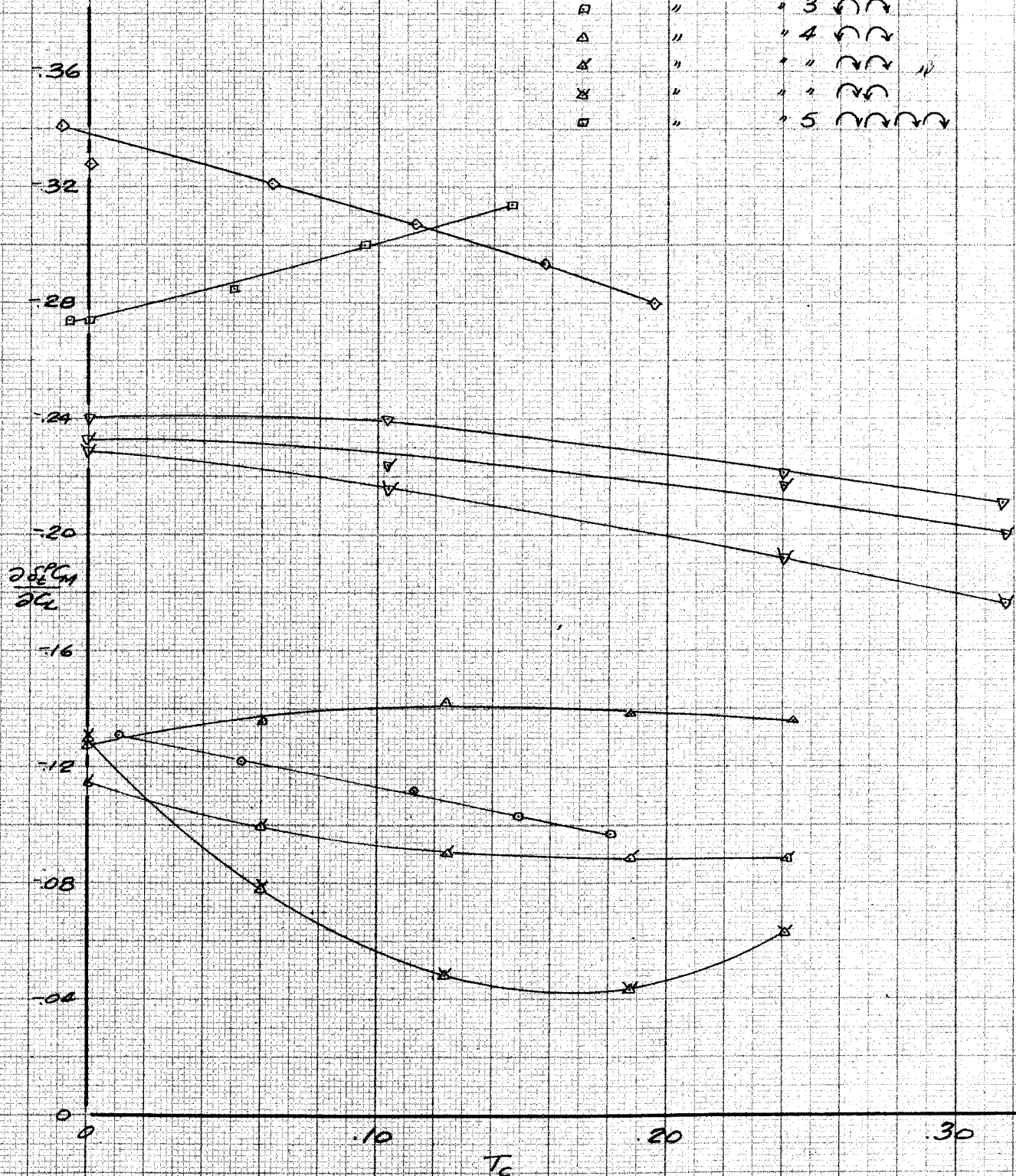
COMPARISON OF STABILIZER EFFECTIVENESS FOR THE FIVE AIRPLANES
AND THREE ROTATIONS

○ AIRPLANE No. 1, ↷
 ▼ " " 2, ↷↷, ↷↷, ↷↷
 □ " " 3, ↷↷
 △ " " 4, ↷↷ ↷↷ ↷↷
 ◇ " " 5, ↷↷ ↷↷ ↷↷

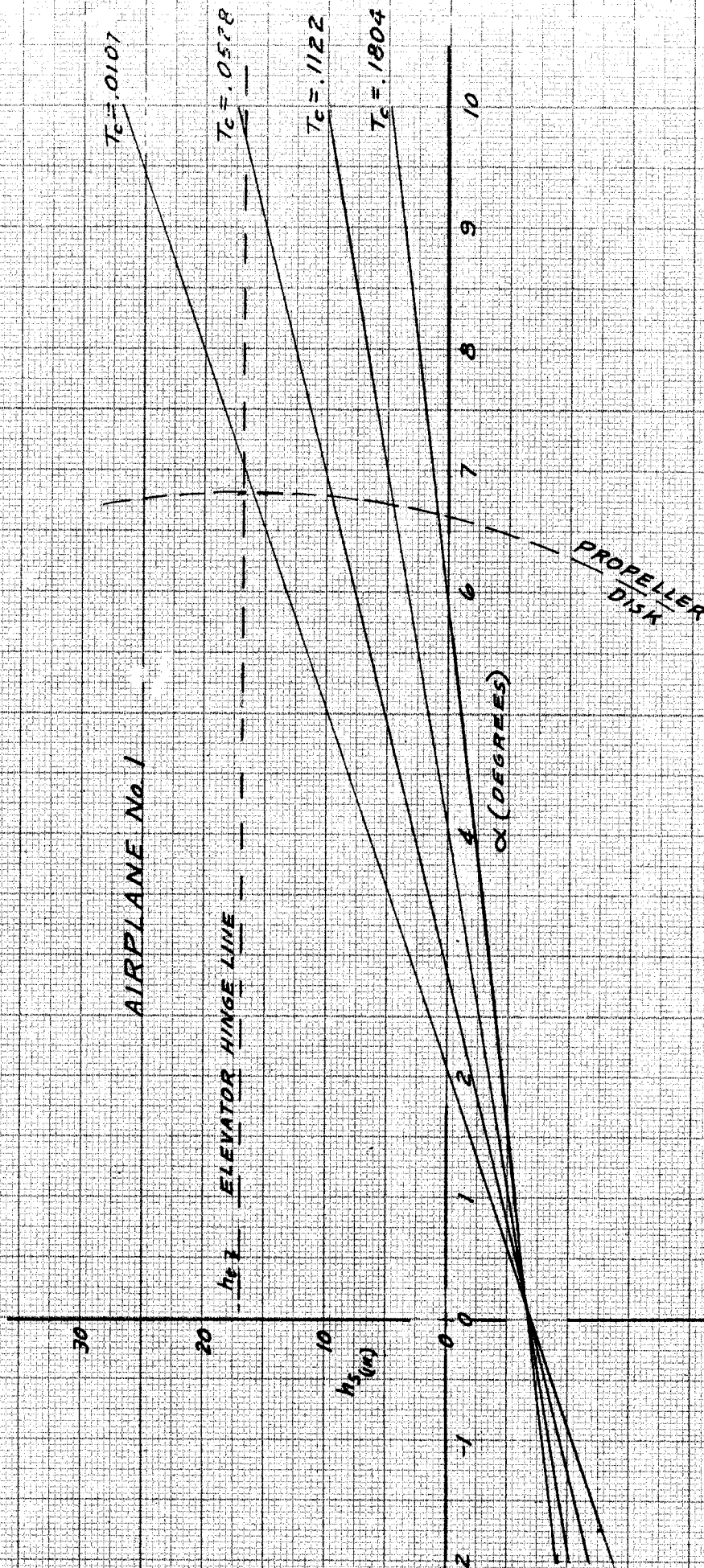


COMPARISON OF $\frac{dip}{dit}$ vs T_c FOR THE FIVE AIRPLANES
AND THREE ROTATIONS

AIRPLANE	No. 1	2	3	4	5
○	○	○	○	○	○
▽	▽	▽	▽	▽	▽
▽	▽	▽	▽	▽	▽
▽	▽	▽	▽	▽	▽
□	□	□	□	□	□
△	△	△	△	△	△
×	×	×	×	×	×
×	×	×	×	×	×
×	×	×	×	×	×

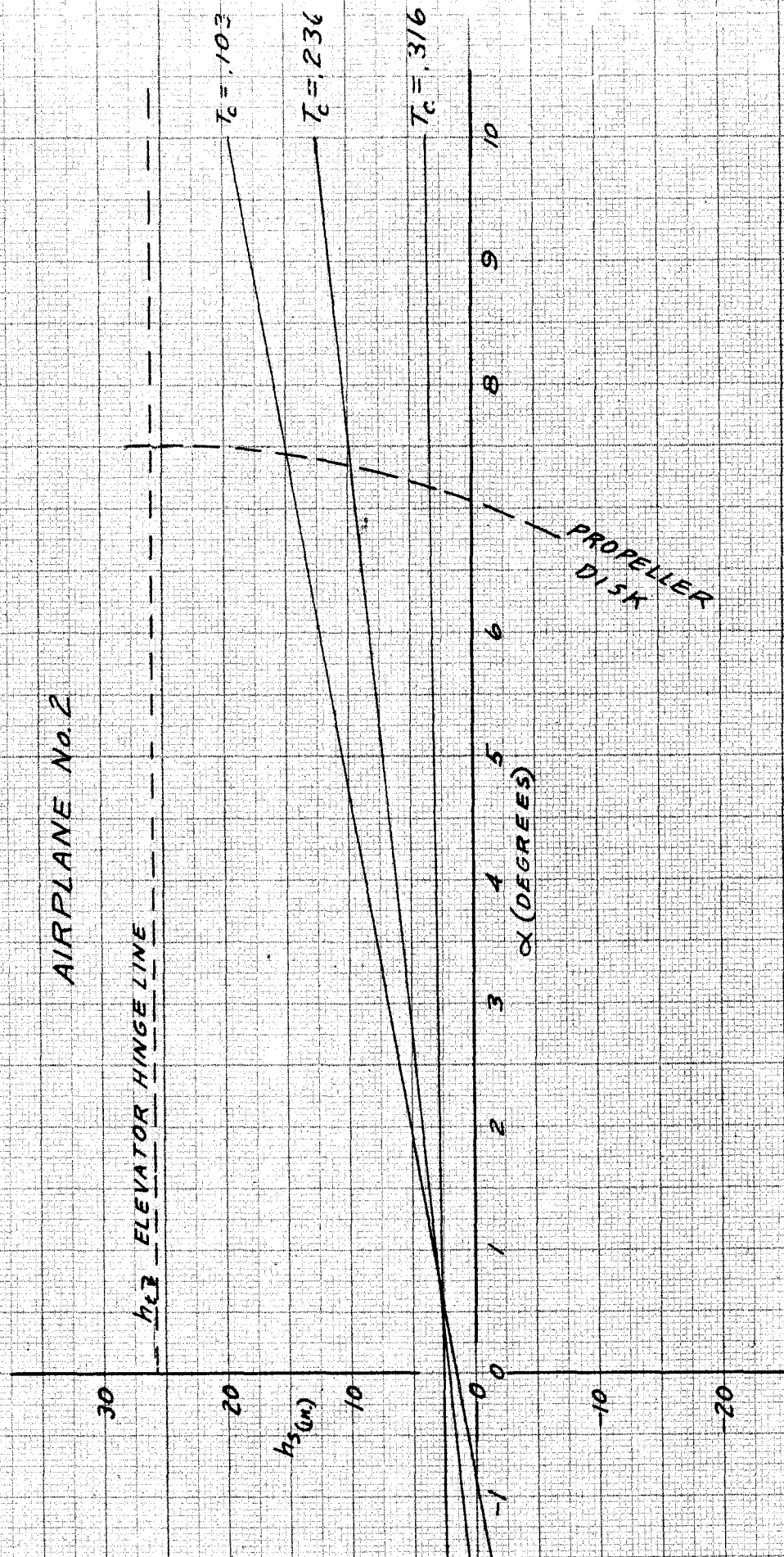


COMPARISON OF TAIL PITCHING MOMENT SLOPES AS A FUNCTION OF T_C
FOR THE FIVE AIRPLANES AND THREE ROTATIONS

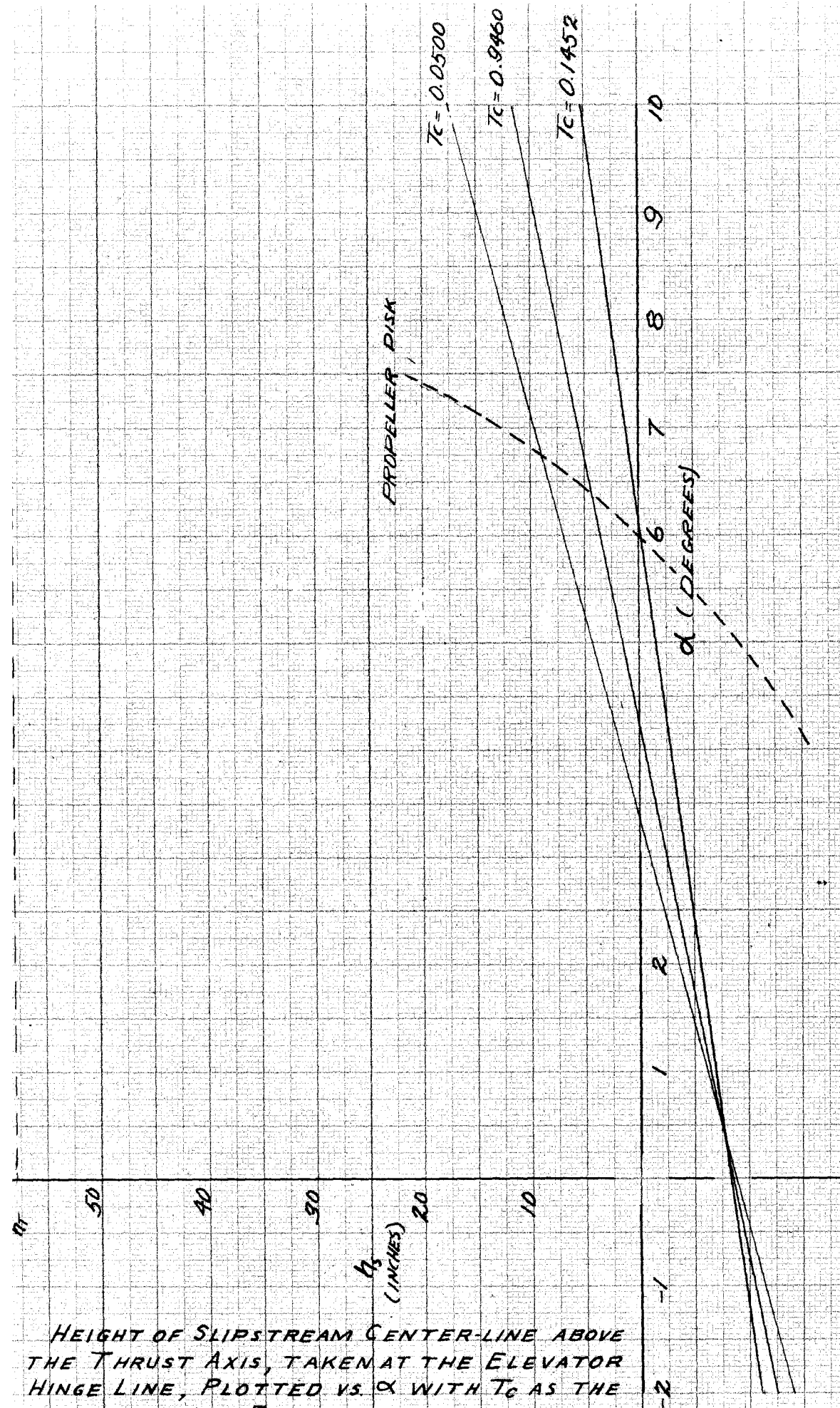


HEIGHT OF SLIPSTREAM CENTER-LINE ABOVE THE THRUST AXIS, TAKEN AT THE ELEVATOR HINGE LINE, PLOTTED VS. α WITH T_c AS THE PARAMETER

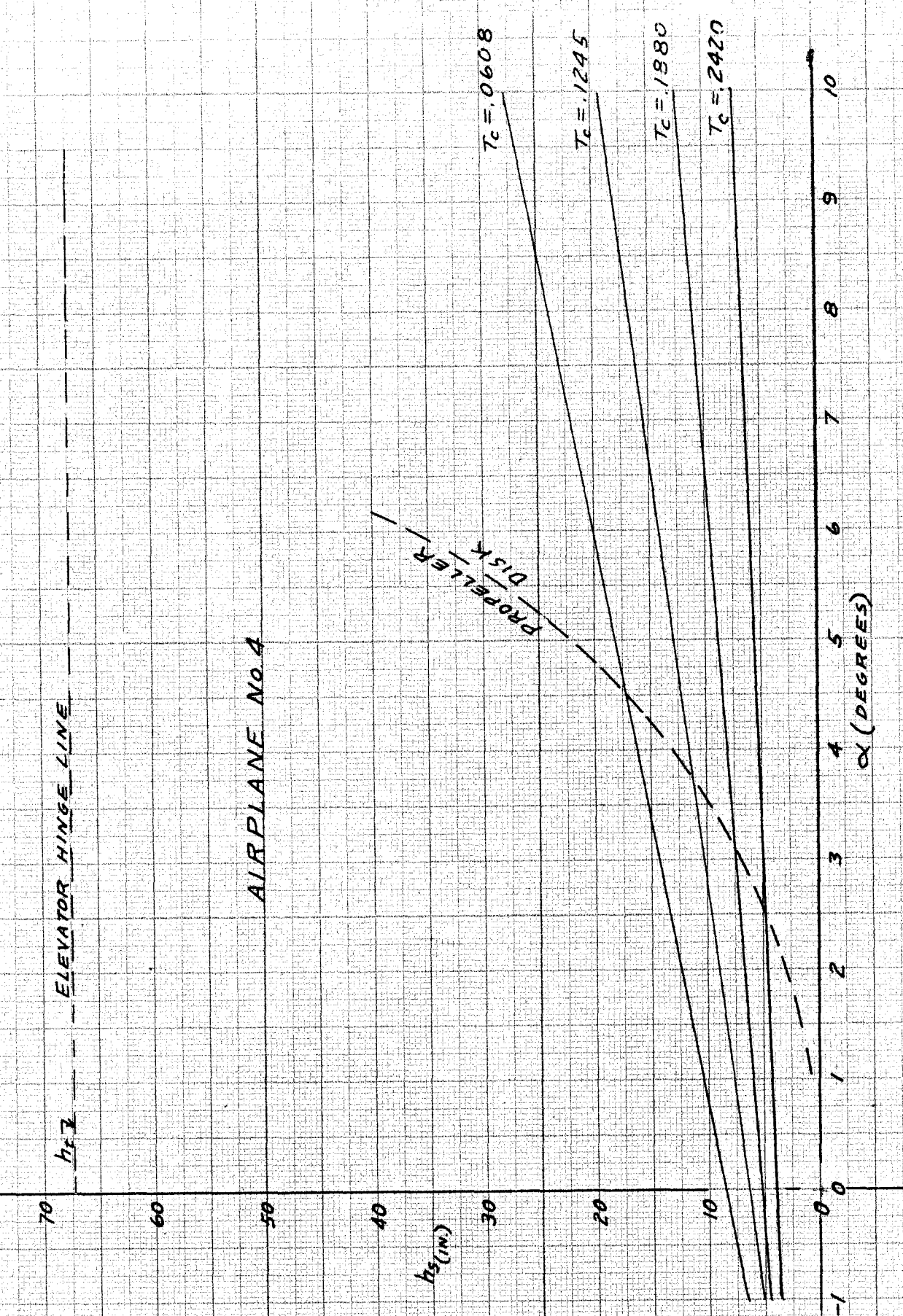
AIRPLANE No. 1



HEIGHT OF SLIPSTREAM CENTER-LINE ABOVE THE THRUST, TAKEN AT THE ELEVATOR HINGE LINE, PLOTTED VS α WITH T_c AS THE PARAMETER FOR AIRPLANE No. 2

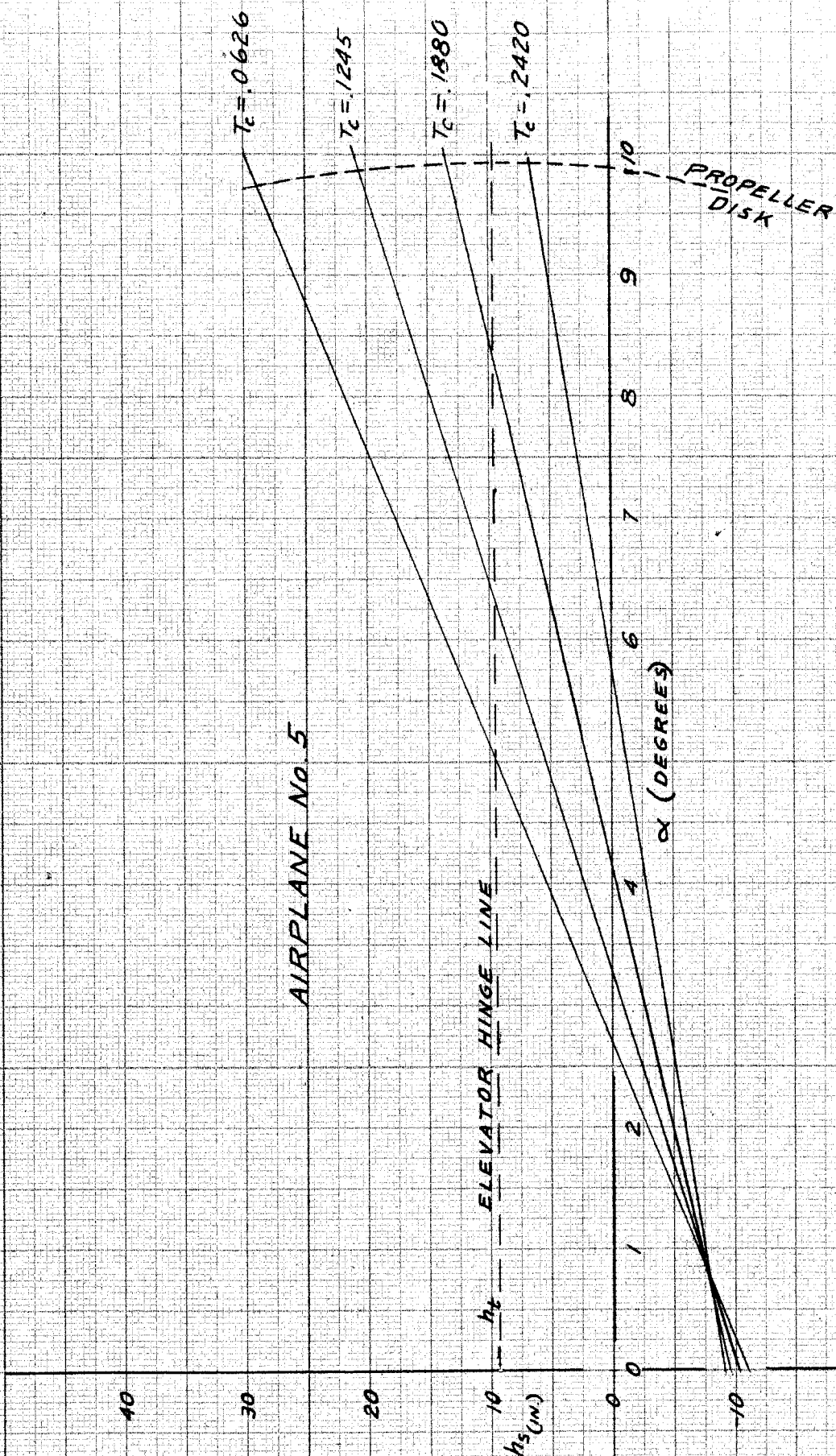


HEIGHT OF SLIPSTREAM CENTER-LINE ABOVE
THE THRUST AXIS, TAKEN AT THE ELEVATOR
HINGE LINE, PLOTTED VS. α WITH T_c AS THE
PARAMETER



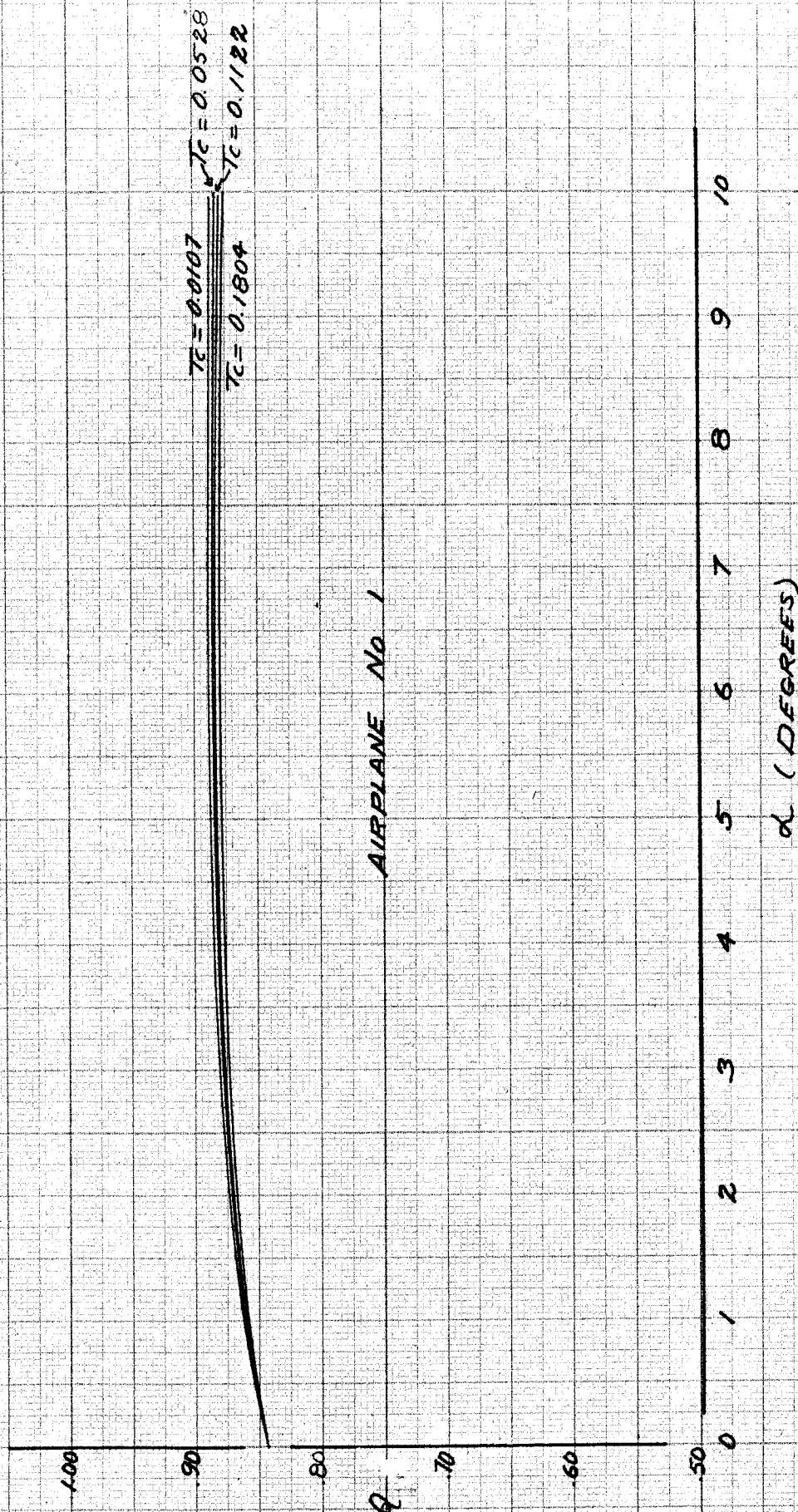
HEIGHT OF SLIPSTREAM CENTER-LINE ABOVE THE THRUST AXIS,
TAKEN AT THE ELEVATOR HINGE LINE, PLOTTED VS. α WITH
 T_c AS THE PARAMETER

AIRPLANE No. 4



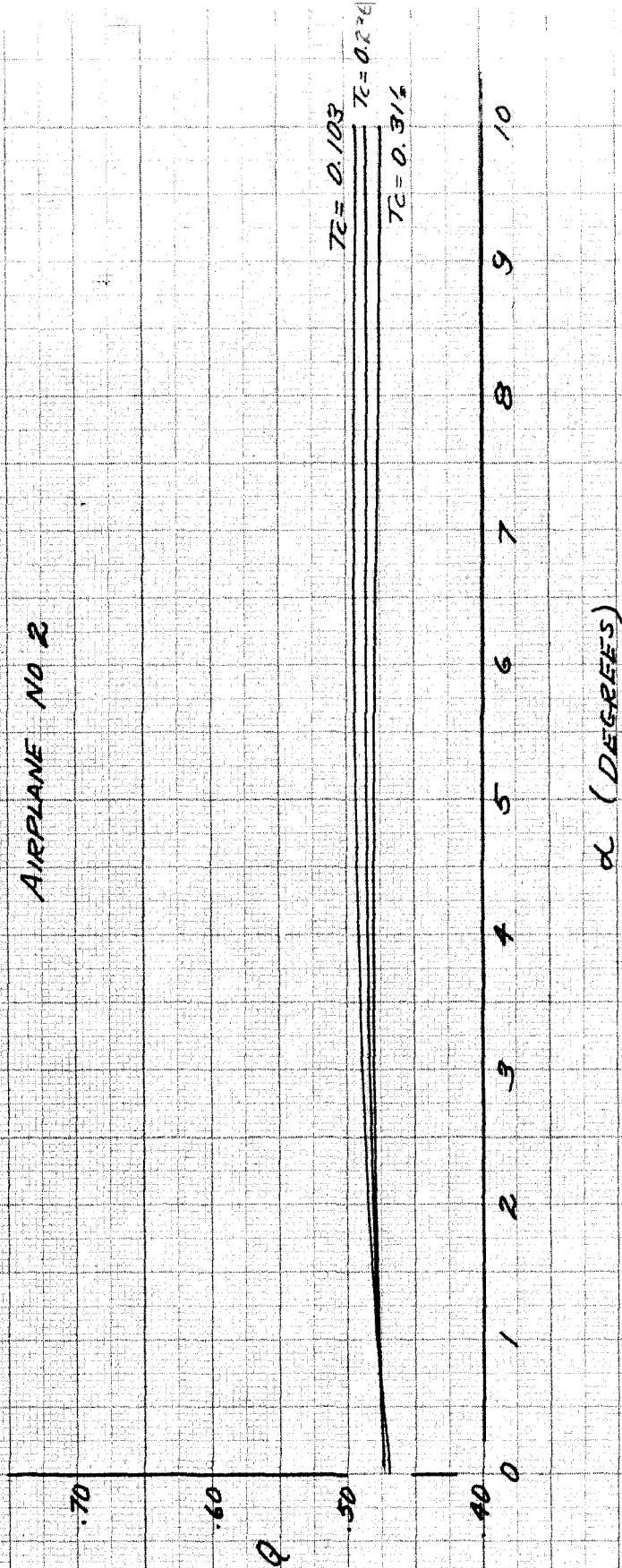
HEIGHT OF SLIPSTREAM CENTER-LINE ABOVE THE THRUST
AXIS, TAKEN AT THE ELEVATOR HINGE-LINE, PLOTTED VS. α WITH
 T_c AS THE PARAMETER

AIRPLANE No. 5



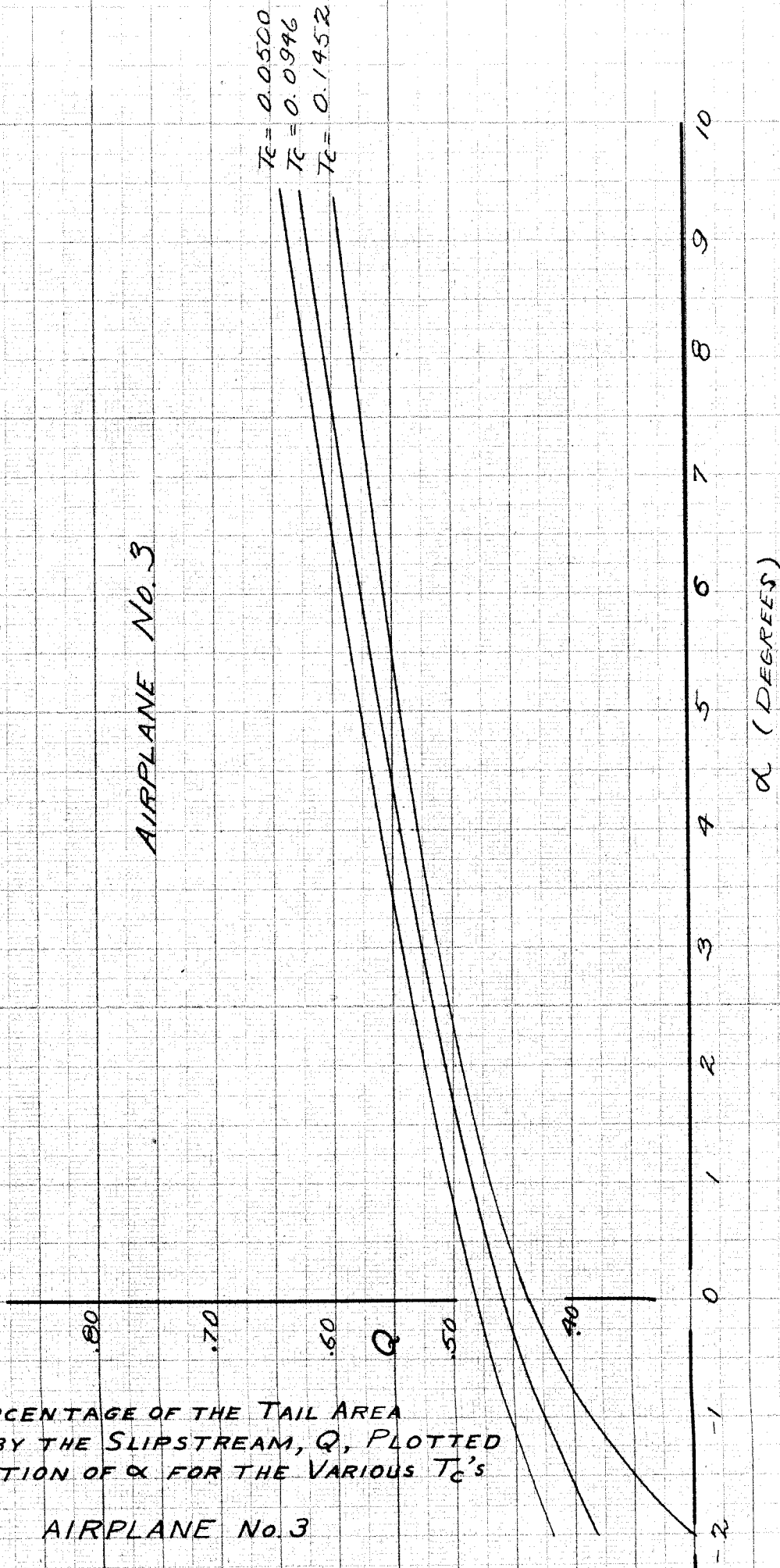
THE PERCENTAGE OF THE TAIL AREA COVERED BY THE SLIPSTREAM, Q , PLOTTED AS A FUNCTION OF α FOR VARIOUS VALUES OF T_c FOR AIRPLANE NO. 1

AIRPLANE NO 2



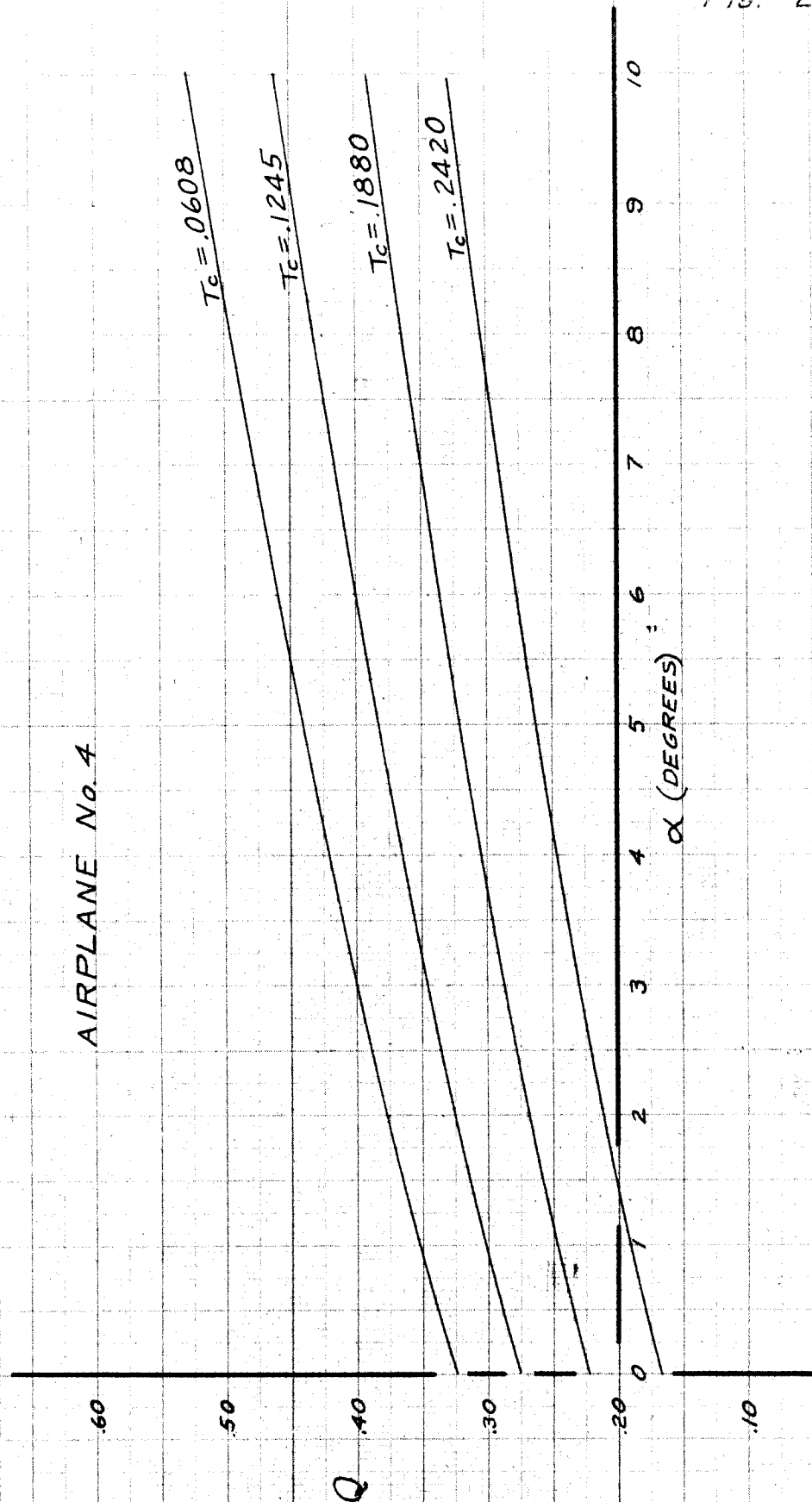
THE PERCENTAGE OF THE TAIL AREA COVERED BY THE SLIPSTREAM, Q , PLOTTED AS A FUNCTION OF α FOR THE VARIOUS VALUES OF TC FOR AIRPLANE NO. 2

AIRPLANE No. 3



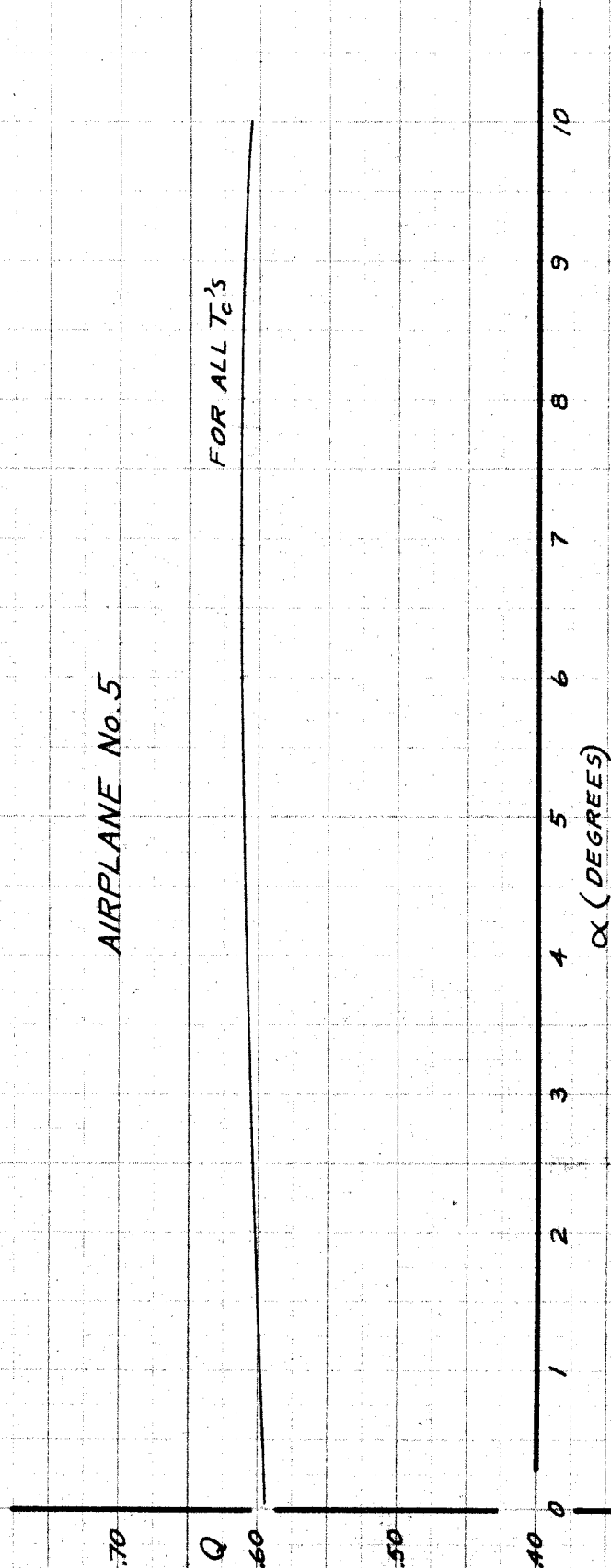
THE PERCENTAGE OF THE TAIL AREA
COVERED BY THE SLIPSTREAM, Q , PLOTTED
AS A FUNCTION OF α FOR THE VARIOUS T_c 's

AIRPLANE No. 3

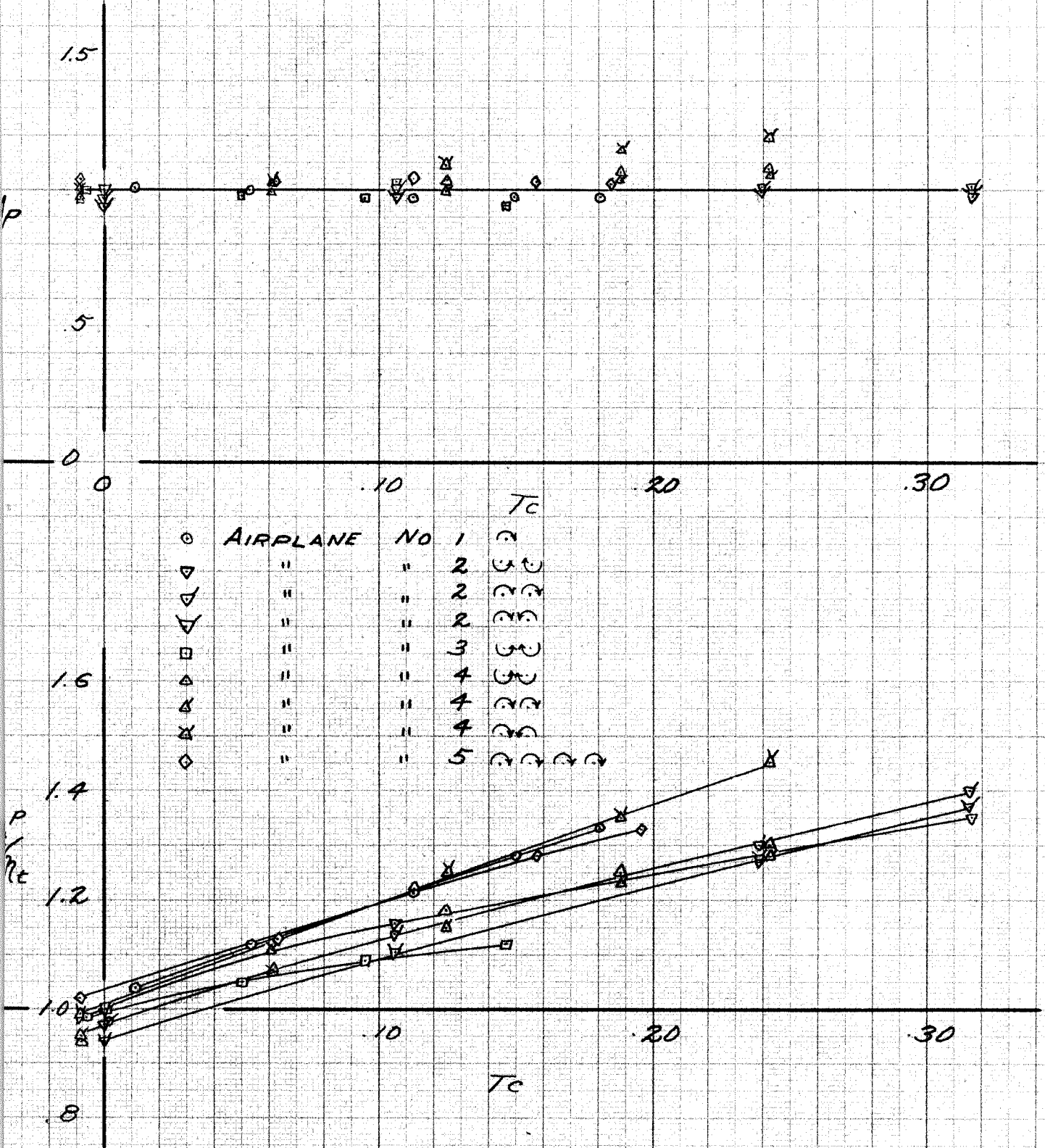


THE PERCENTAGE OF THE TAIL AREA COVERED BY THE SLIPSTREAM, Q , PLOTTED AS A FUNCTION OF α FOR THE VARIOUS T_c 's

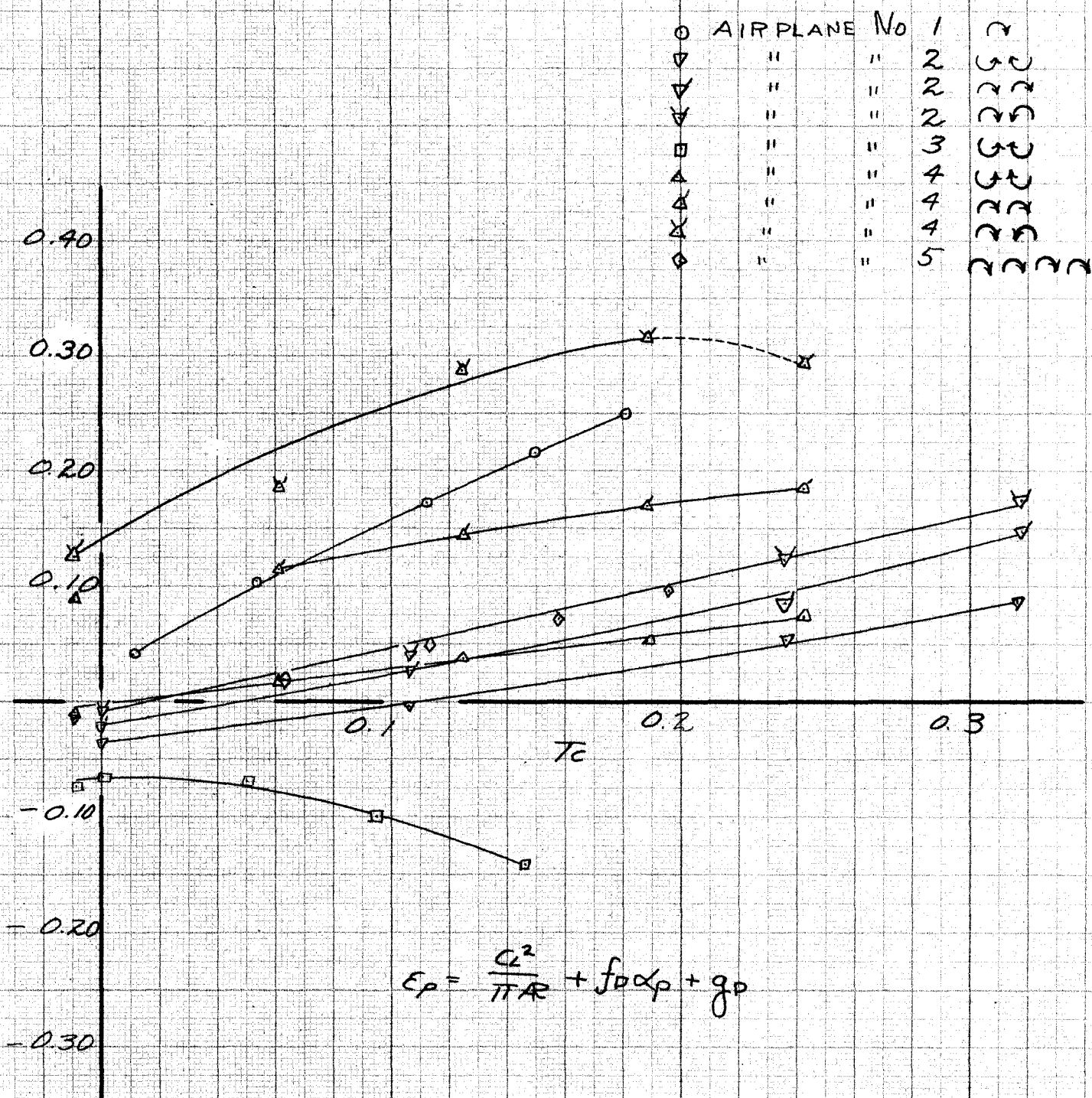
AIRPLANE No. 4



THE PERCENTAGE OF THE TAIL AREA COVERED BY THE
SLIPSTREAM, Q, PLOTTED AS A FUNCTION OF α
FOR THE VARIOUS T_c 's
AIRPLANE No. 5

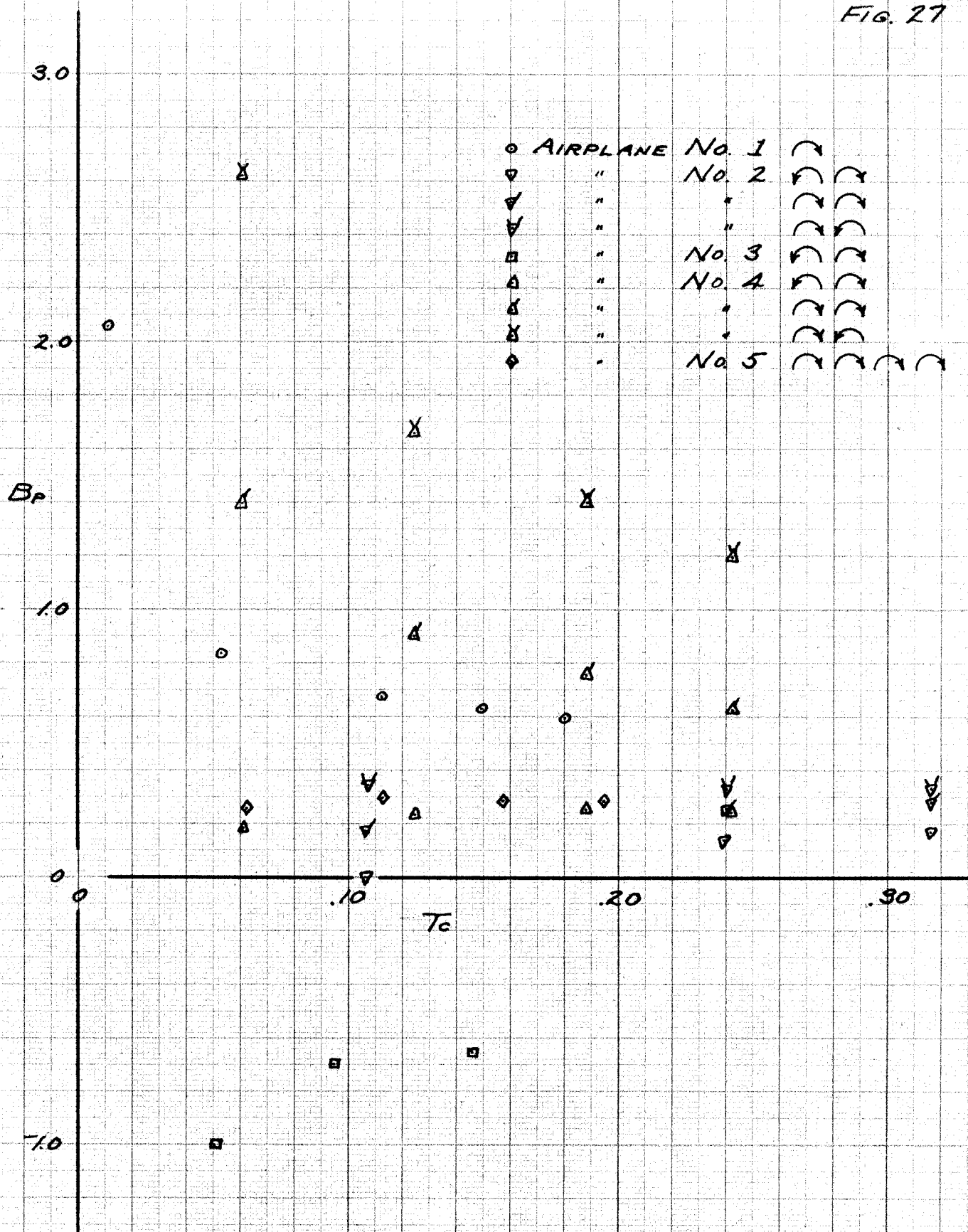


THE VARIATION WITH THRUST OF $\frac{P}{P_t}$ AND A_p FOR THE FIVE AIRPLANES AND THREE ROTATIONS



$$E_p = \frac{C_L^2}{\pi A} + f_D \alpha_p + g_D$$

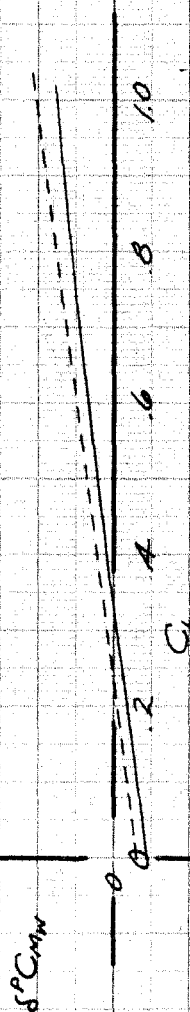
THE VARIATION WITH THRUST OF THE DOWNWASH INCREMENT
DUE TO POWER, FOR FIVE AIRPLANES AND THREE ROTATIONS



THE VARIATION OF B_p WITH T_c FOR THE FIVE AIRPLANES AND THREE ROTATIONS

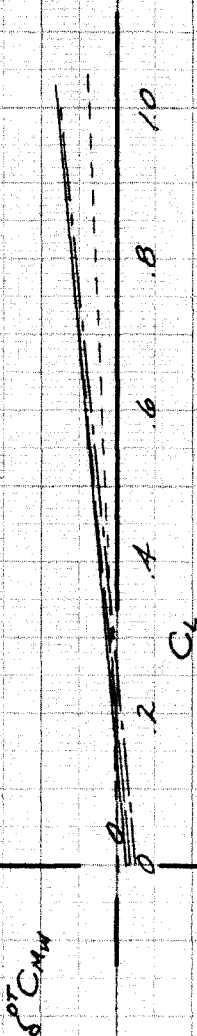
AIRPLANE No 1, $T_c = 0.007$

— P_R , \bigcirc , EXPERIMENTAL
--- CALCULATED



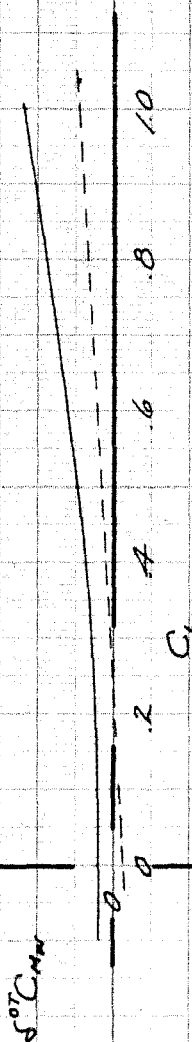
AIRPLANE No 2, ZERO THRUST

— P_L , P_R , \bigcirc , EXPERIMENTAL
--- P_R , \bigcirc , " "
--- P_R , \bigcirc , " "
--- CALCULATED



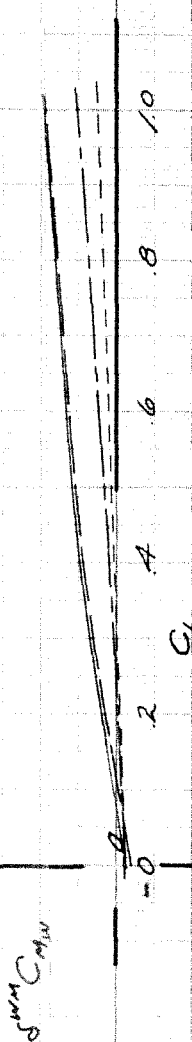
AIRPLANE No 3, ZERO THRUST

— P_L , P_R , \bigcirc , EXPERIMENTAL
--- CALCULATED



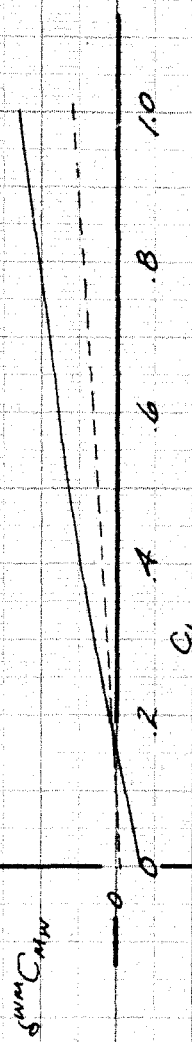
AIRPLANE No 4, WINDMILLING

— P_R , P_R , \bigcirc , EXPERIMENTAL
--- P_R , \bigcirc , " "
--- P_L , P_R , \bigcirc , " "
--- CALCULATED



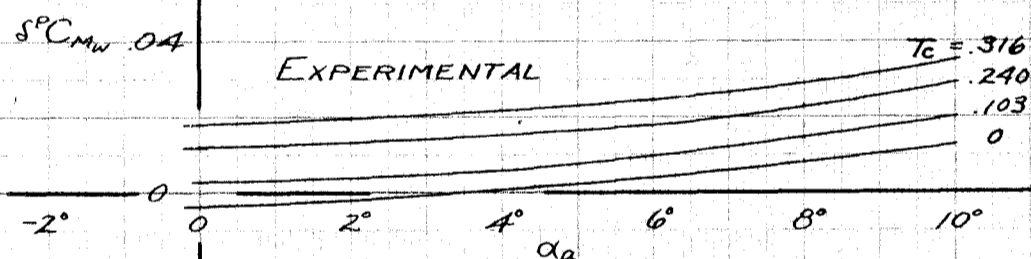
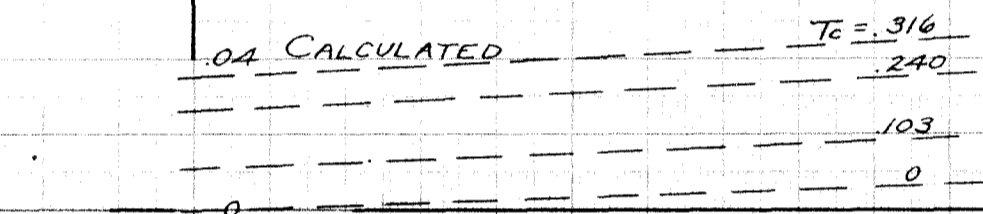
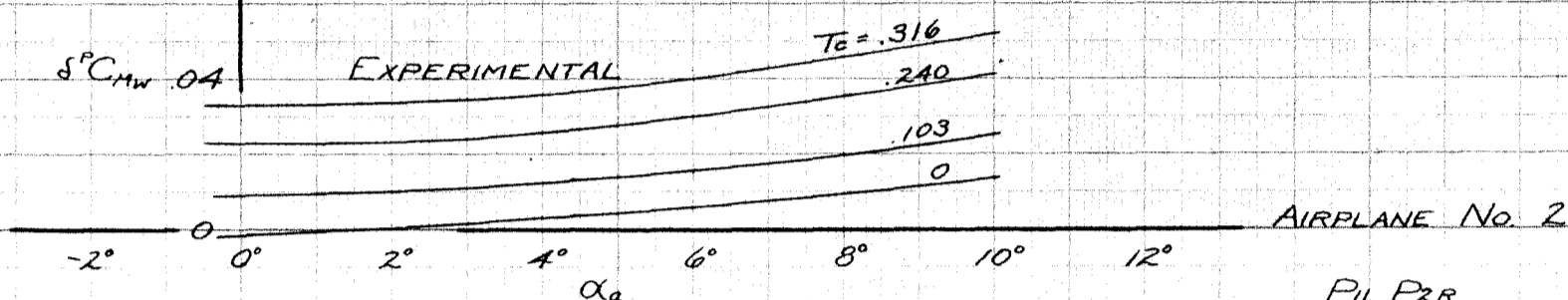
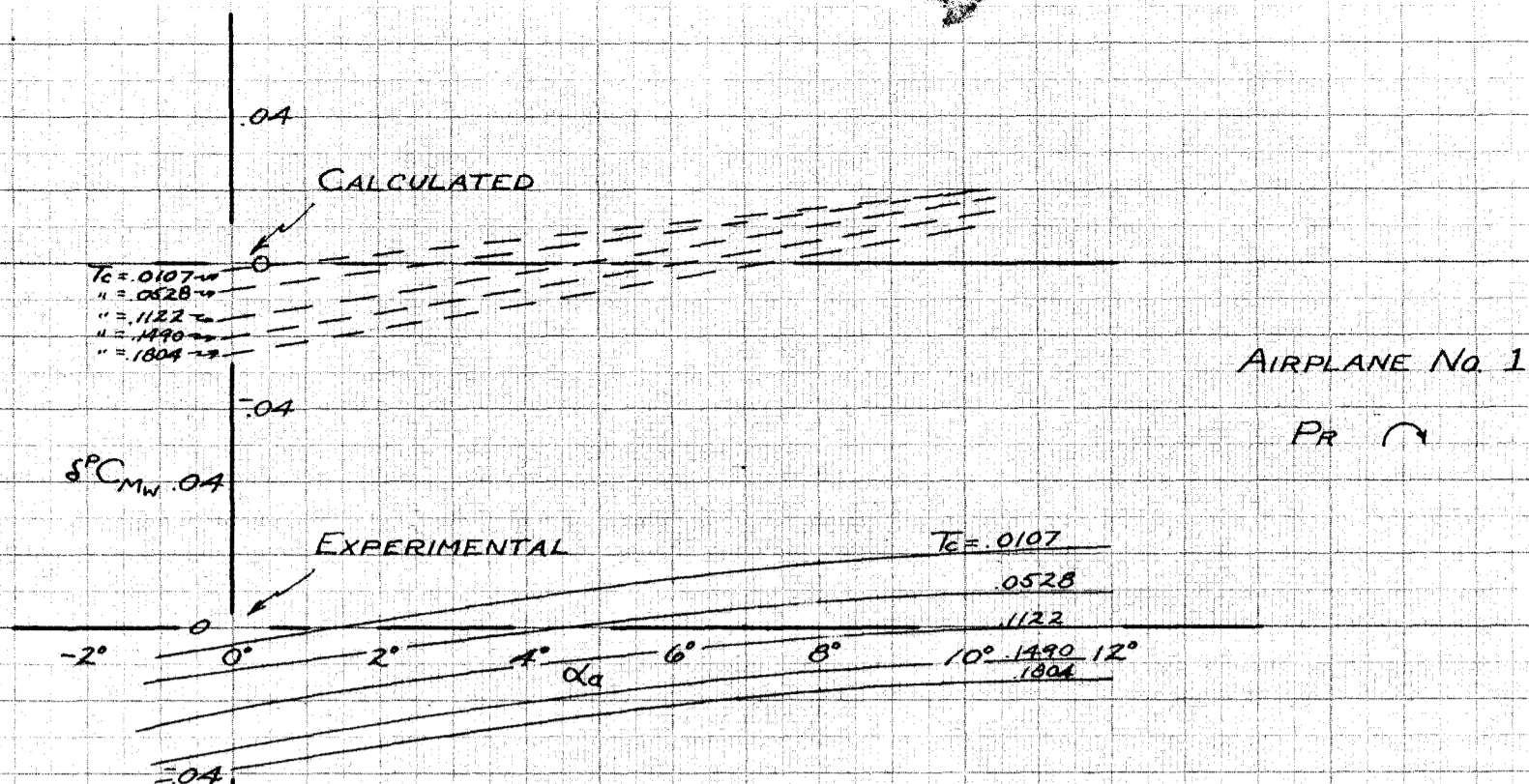
AIRPLANE No 5, WINDMILLING

— P_R , P_R , P_R , \bigcirc , EXPERIMENTAL
--- CALCULATED



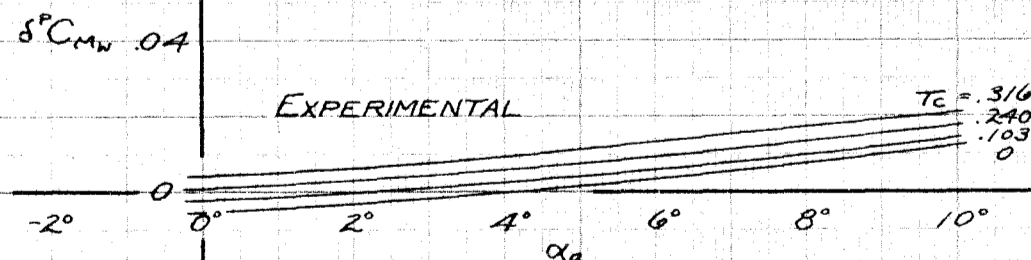
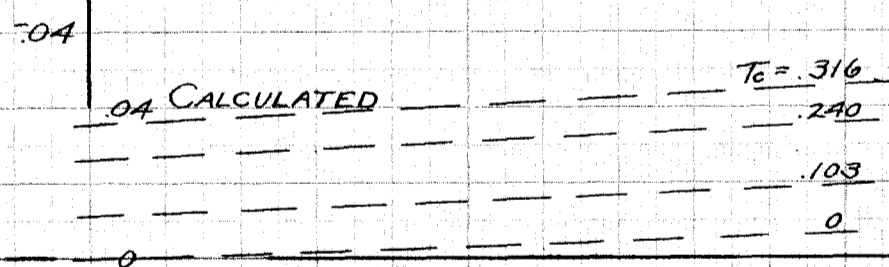
EXPERIMENTAL AND CALCULATED VALUES OF THE
PITCHING MOMENT INCREMENT DUE TO PROPELLER
ROTATION FOR THE TAIL REMOVED CONFIGURATION

EXPERIMENTAL AND CALCULATED VALUES OF $\delta^P C_{Mw}$,
THE PITCHING MOMENT INCREMENT DUE TO POWER,
TAIL REMOVED, FOR AIRPLANES 1 AND 2 AND THREE
ROTATIONS



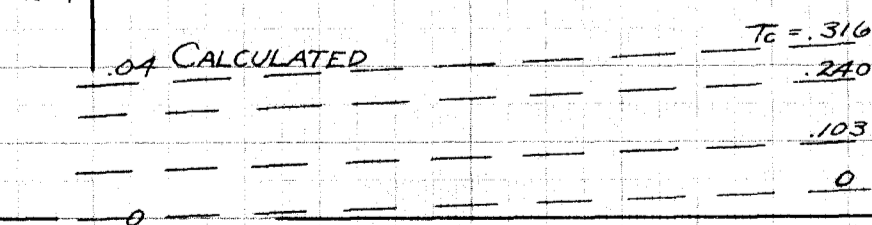
AIRPLANE No. 2

PIL P2R \curvearrowright

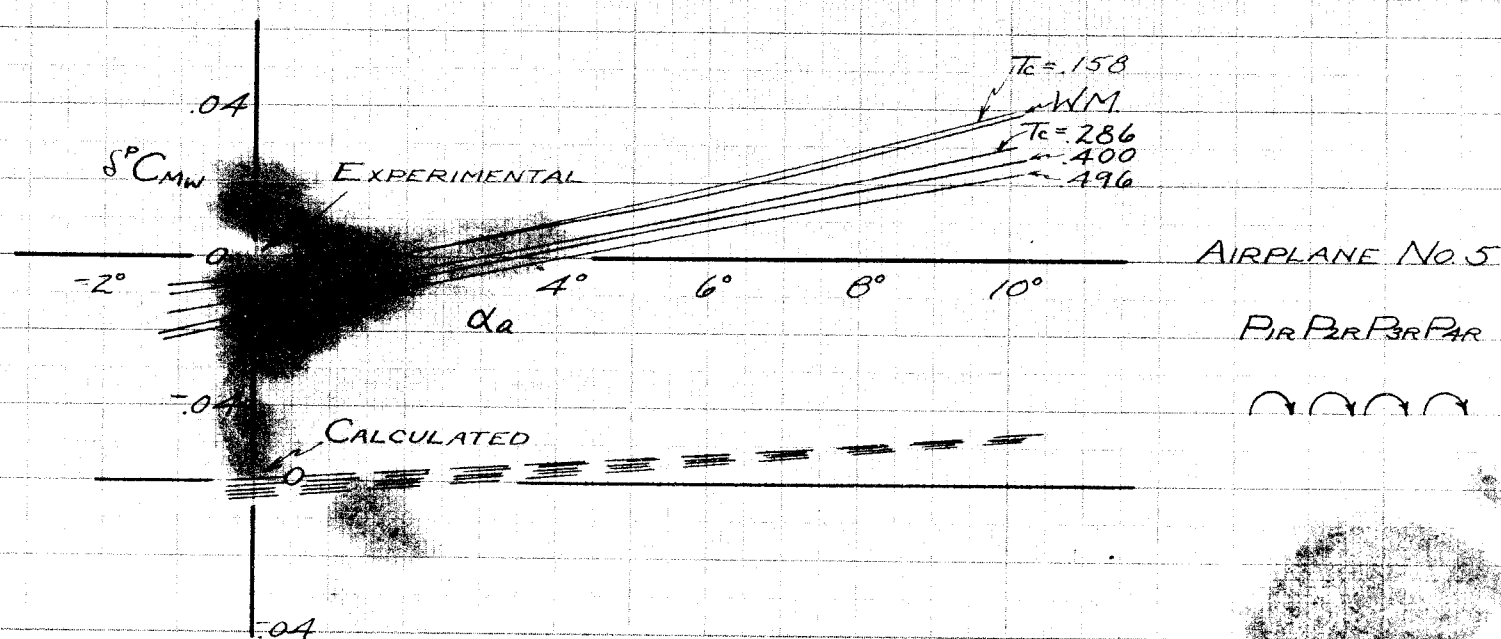
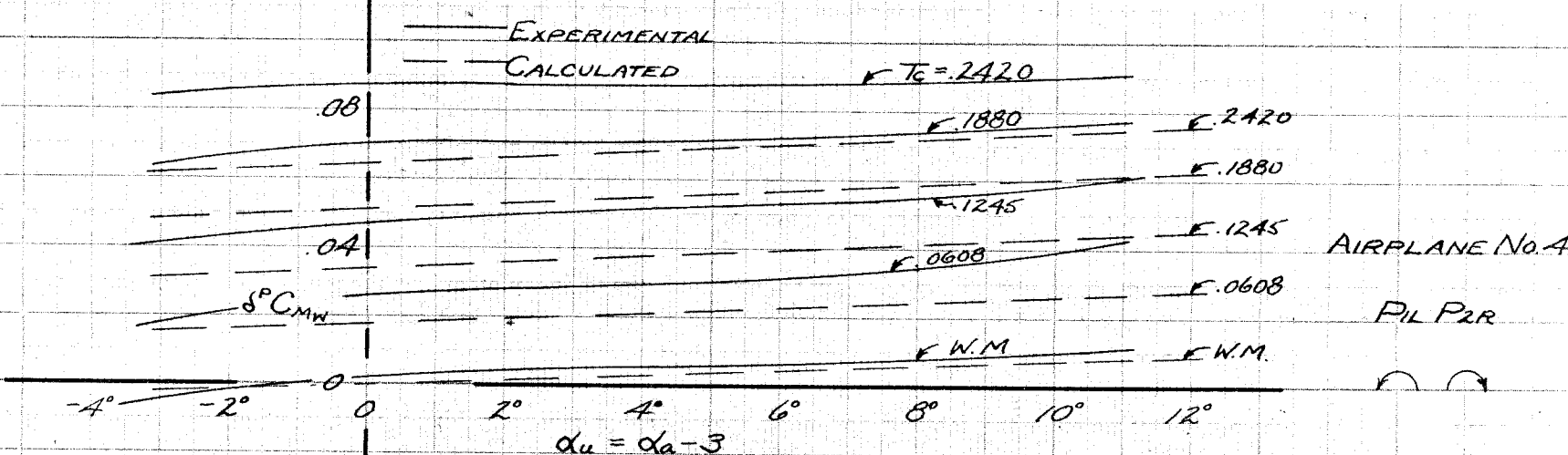
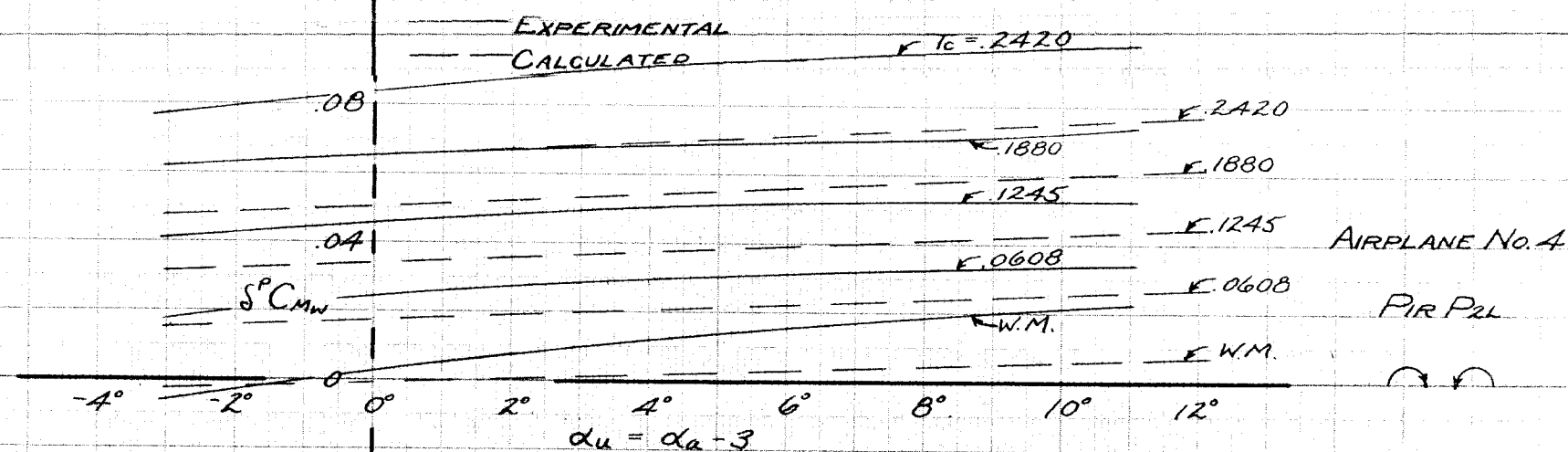
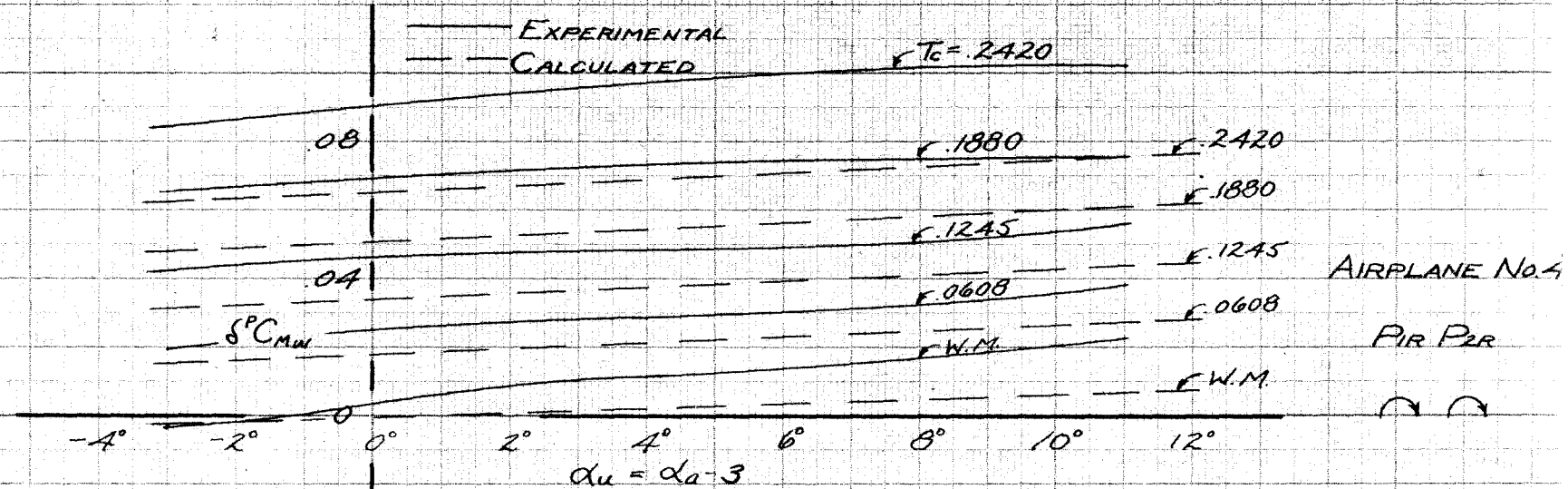
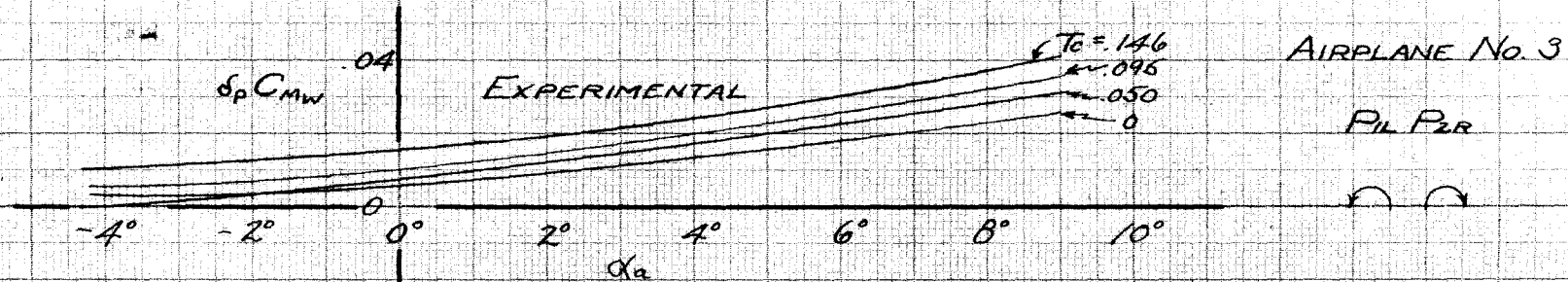


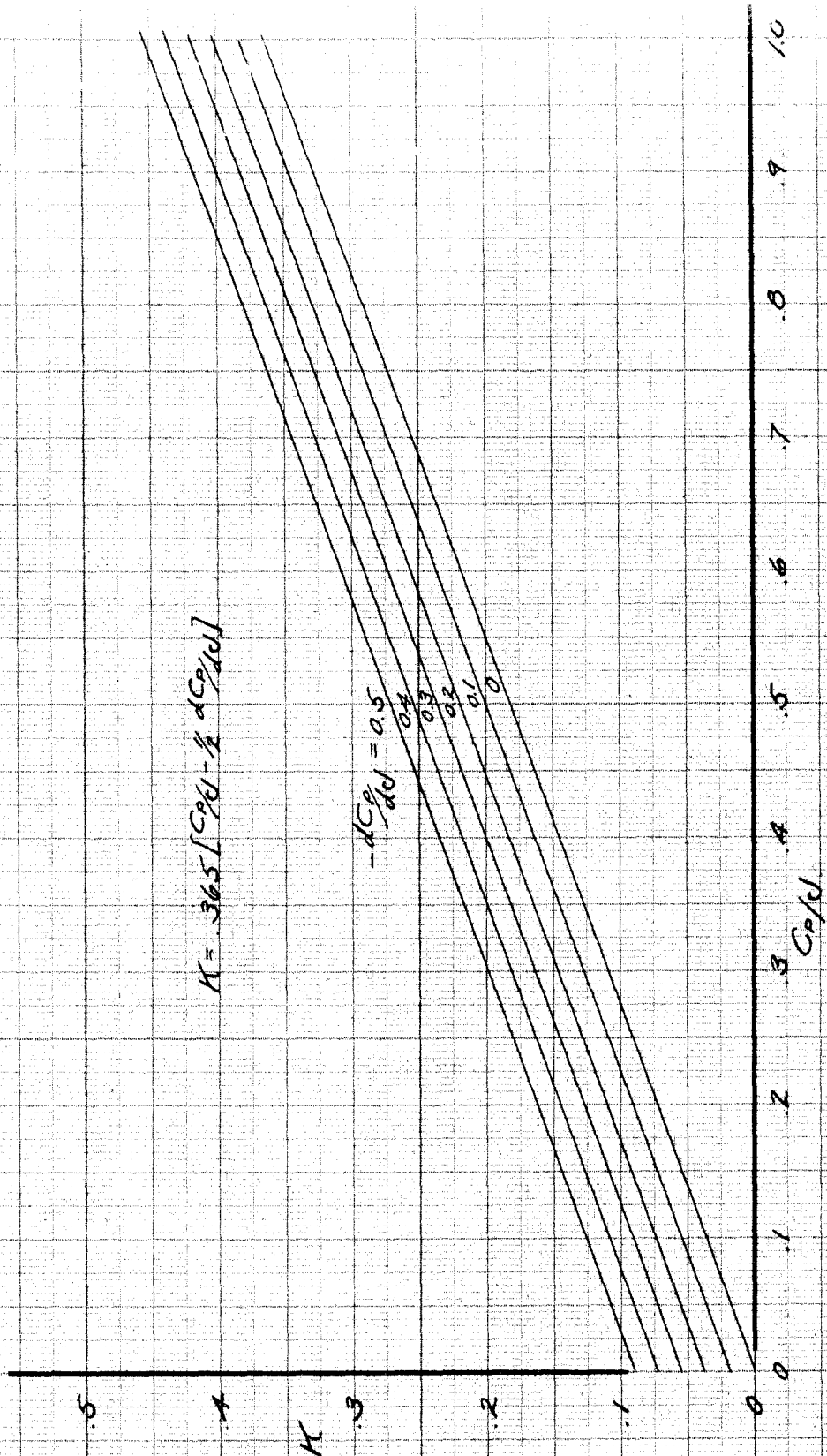
AIRPLANE No. 2

PIL P2L \curvearrowright



EXPERIMENTAL AND CALCULATED VALUES OF $\delta^p C_{MW}$, THE
PITCHING MOMENT INCREMENT DUE TO POWER, TAIL REMOVED,
FOR AIRPLANES 3, 4, AND 5 AND THREE ROTATIONS

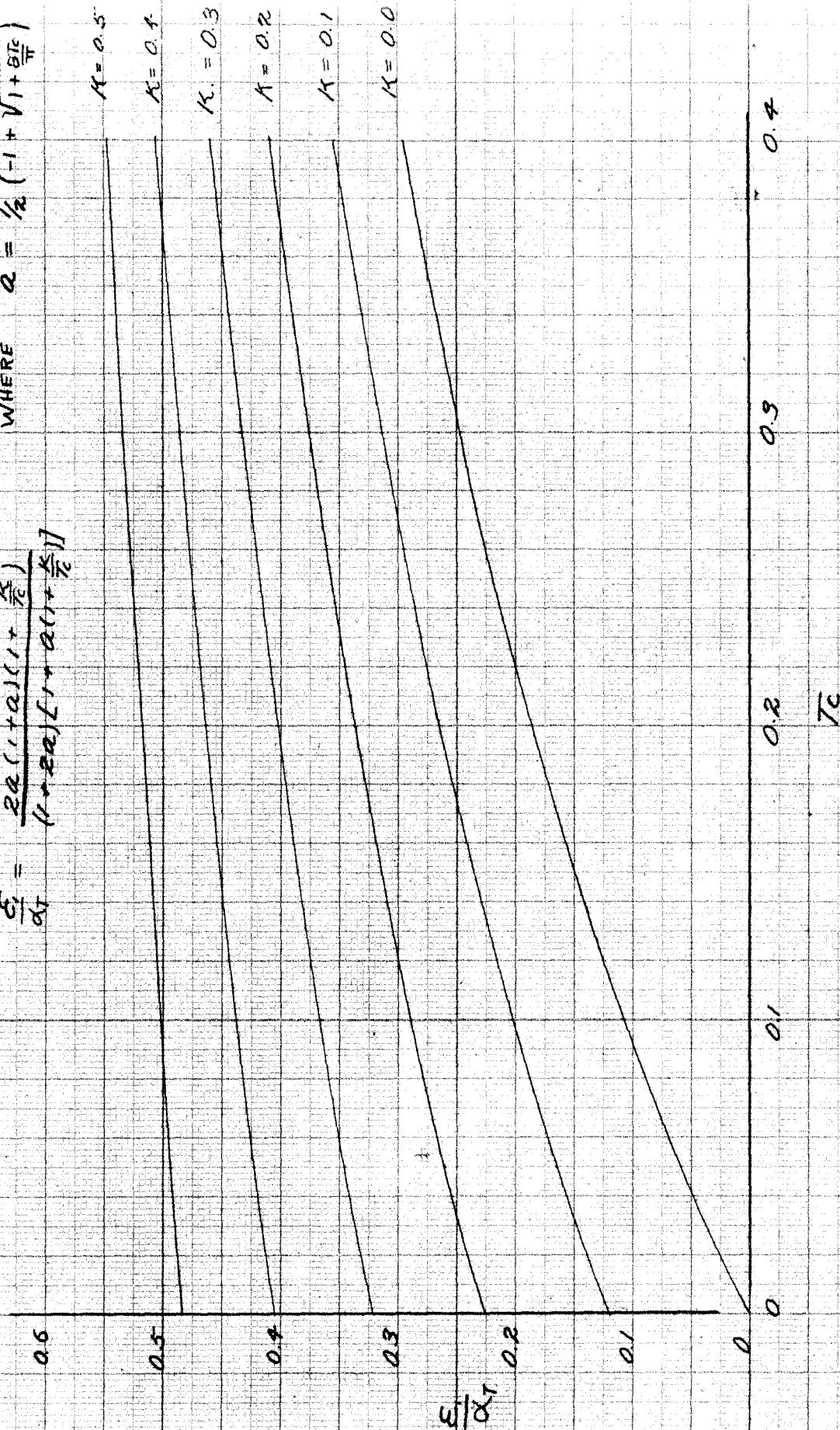




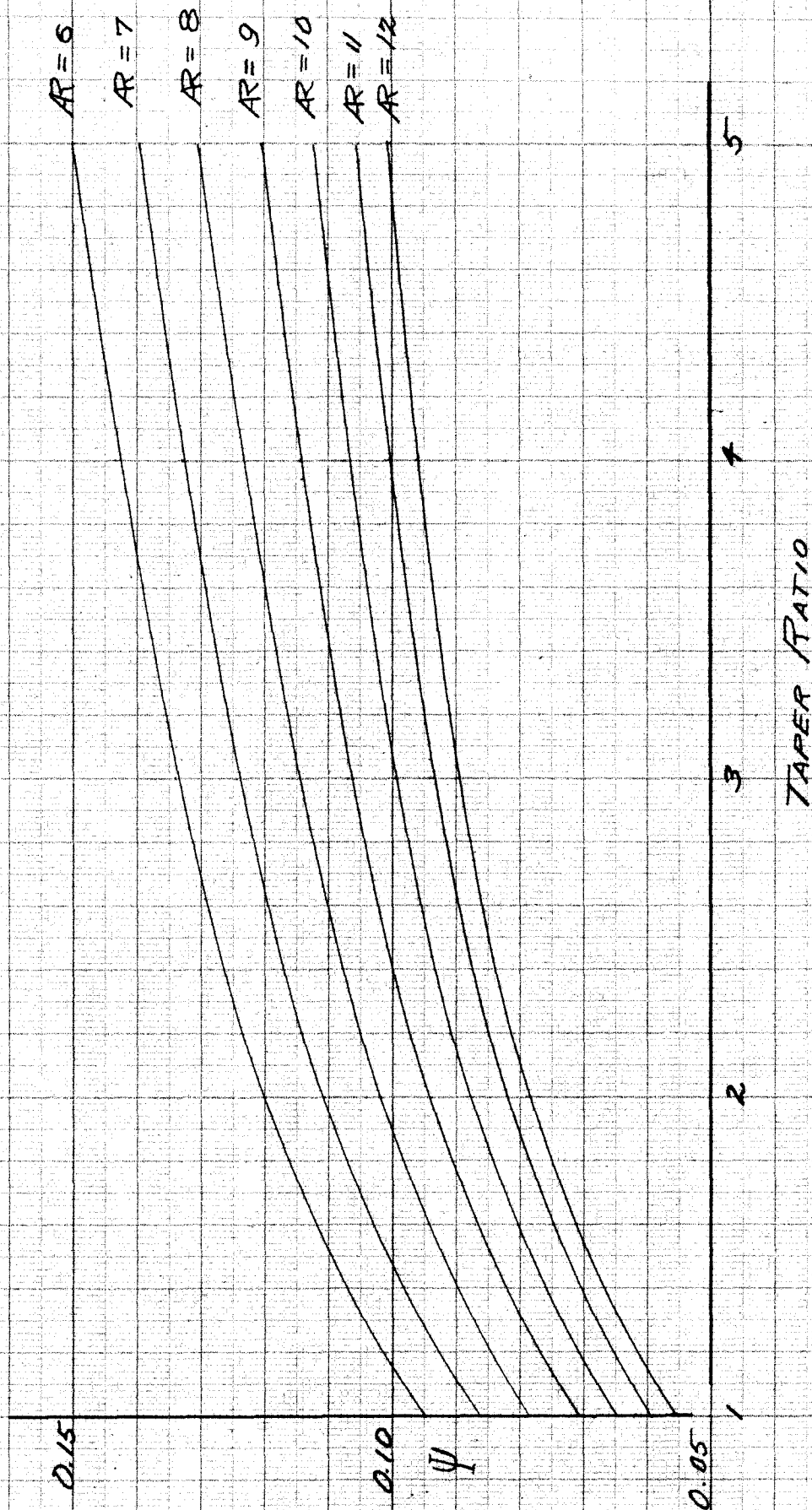
THE PROPELLER NORMAL FORCE FUNCTION, K , PLOTTED
VERSUS Cp/d FOR VARIOUS VALUES OF dCp/d

WHERE $Q = \frac{1}{2}(-1 + \sqrt{1 + \frac{8T_c}{\pi}})$

$$\frac{E}{\alpha_T} = \frac{2a(1+a)(1+\frac{K}{T_c})}{(1+2a)f(a(1+\frac{K}{T_c}))}$$

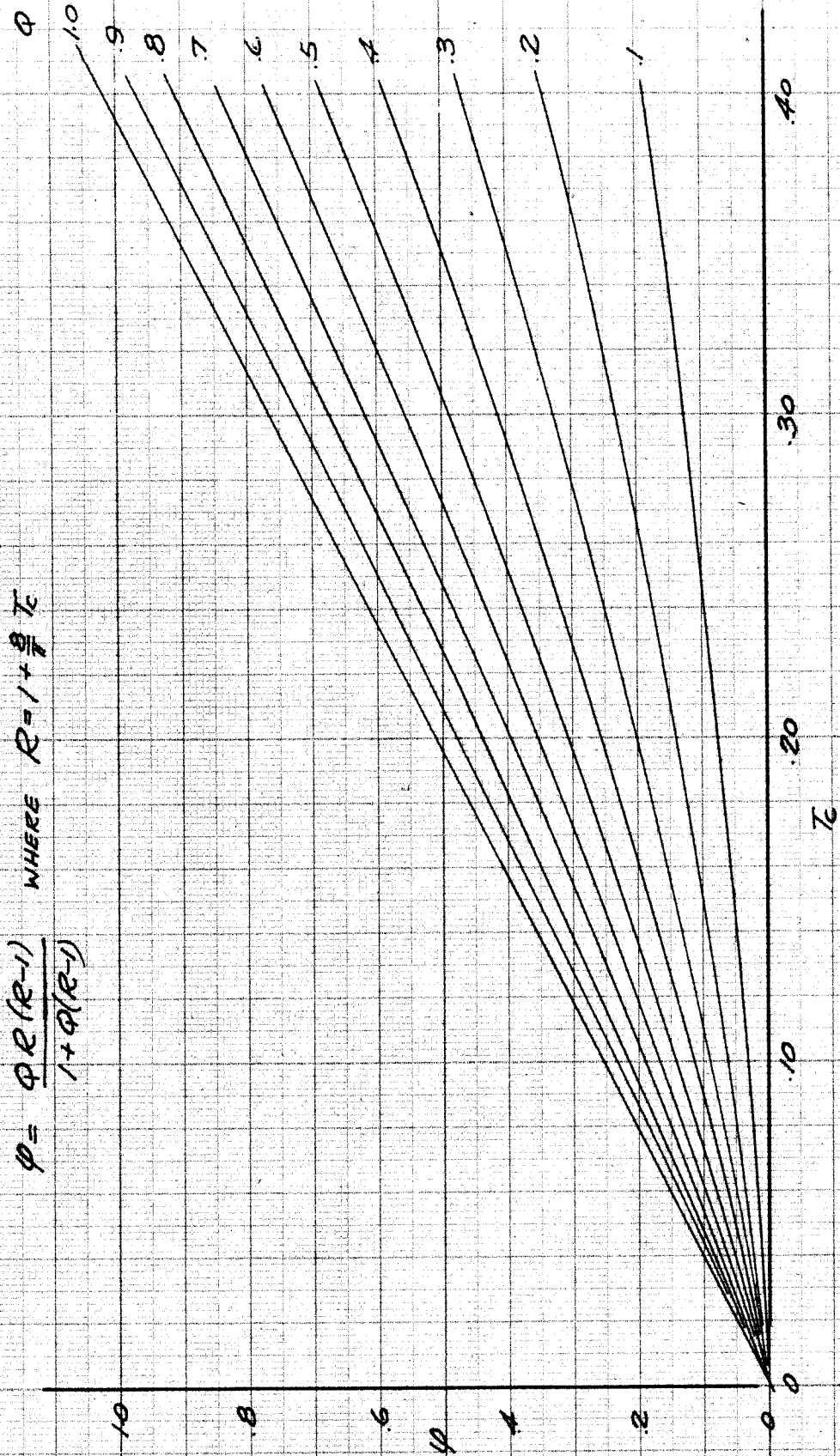


THE FORM OF THE FUNCTION $\frac{E}{\alpha_T}$

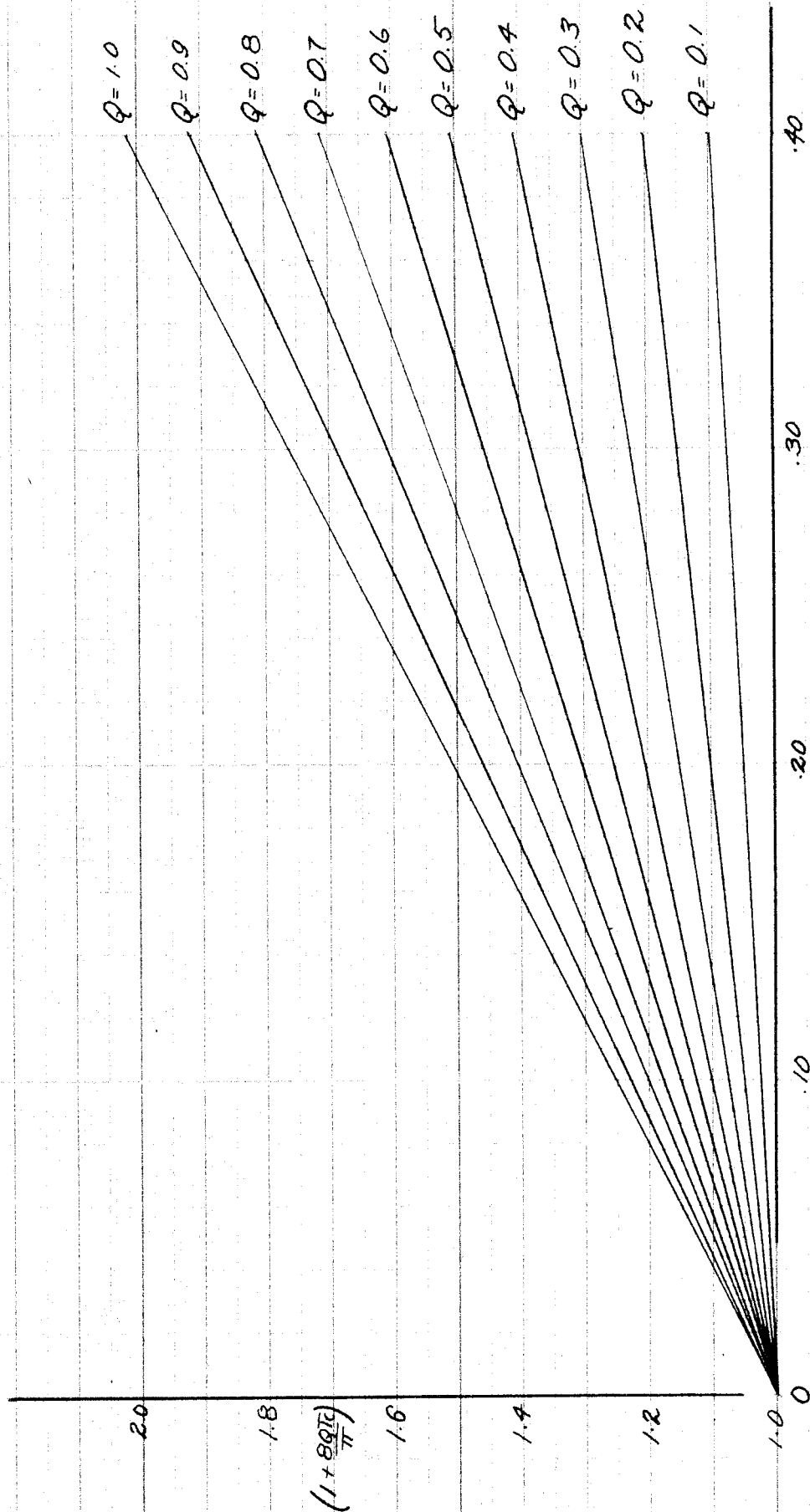


THE FORM OF FUNCTION III

DATA FROM TECH REPORT NO. 648



THE FORM OF THE FUNCTION ϕ



THE FORM OF THE FUNCTION $\frac{(1 + BQTe)}{\pi}$